COLUMBIA ACCIDENT INVESTIGATION BOARD (CAIB)/ NATIONAL AERONAUTICS AND SPACE ADMINISTRATION (NASA) ACCIDENT INVESTIGATION TEAM (NAIT)

WORKING SCENARIO

FINAL VERSION: JULY 8, 2003

PREFACE

This Working Scenario report was written to document the collection of known facts, events, timelines, and historical information of particular interest to the final flight of Columbia. The report was written with the understanding that it could be published, either in part or in its entirety, as part of the official Columbia Accident Investigation Board (CAIB) report. The report includes information and results from numerous analyses, tests, and simulations related to the Columbia investigation that have been completed, or were ongoing at the time that this report was completed. It is anticipated that additional analytical and test results will emerge from ongoing work, as well as from future activities associated with the Columbia investigation and efforts related to the Return-To-Flight work. This Working Scenario includes information and results as they existed up to and including July 8, 2003.

CONTENTS

Section **Page**

Section **Page**

Appendix

TABLES

FIGURES

Figure **Page**

Figure **Page**

Figure **Page**

Figure **Page**

Figure **Page**

1.0 INTRODUCTION

1.1 SCOPE

The Working Scenario is the result of a joint effort between the Columbia Accident Investigation Board (CAIB) and the NASA Accident Investigation Team (NAIT). This effort collates and documents the principal facts related to specific vehicle element events, timelines, and data. It also includes pertinent historical data surrounding some of the key vehicle element considerations in the investigation. The scenario addresses the chronology of vehicle events from prelaunch, Launch Countdown (LCD), launch/ascent, orbit, and entry as well as specific information for the External Tank (ET) and the Left Hand (LH) wing, including aspects of the Reinforced Carbon-Carbon (RCC) and attachment hardware. Vehicle processing and significant preflight events and milestones are also discussed. The scenario addresses technical aspects only, and does not address management practices or philosophies, or other organizational considerations.

The chronological portion of the scenario is contained in Sections 2 through 5 of this report. These sections discuss the prelaunch, launch, orbit, and deorbit/entry portions of the Space Transportation System 107 mission (STS-107). Sections 6 through 8 address the facts related to the Reusable Solid Rocket Motor (RSRM), Solid Rocket Booster (SRB), and Space Shuttle Main Engine (SSME) elements. Section 9 addresses relevant environmental factors such as weather and age of the ET. Section 10 addresses the details of Columbia vehicle processing, specifically as it pertains to the LH wing, from the most recent Orbiter Major Maintenance (OMM) at Palmdale, California, through the processing for STS-107. This section also includes a number of design and historical considerations for the LH wing and for the RCC in general. Section 11 addresses several aspects of the ET, including manufacturing, Kennedy Space Center (KSC) processing, Thermal Protection System (TPS) requirements, and numerous aspects of the foam insulation. These discussions provide the history of the bipod foam ramp design, fabrication, testing, and address the details of bipod foam ramp debris failure modes, testing, and analyses. Section 12 briefly summarizes the discussion of the working scenario.

The data sources and types include, but are not limited to, telemetry from all flight phases, Modular Auxiliary Data System (MADS) data from ascent and entry, video and imagery from launch/ascent and entry, and launch/ascent radar. It also includes reconstructed aerodynamic and vehicle loads, Radar Cross Section (RCS) and ballistics, aero/thermal, structural, debris forensics, post-flight test data (TPS impact, ET/SRB bolt catcher, wind tunnel, etc.), and prelaunch processing.

1.2 MISSION BACKGROUND

STS-107 was the 113th mission in the Space Shuttle program and Columbia's 28th trip into space. These 28 missions spanned 22 years with the first being STS-1, launched on April 12, 1981. The STS-107 mission was a science research mission and the payload complement consisted of the Spacehab Double Research Module and the Fast Reaction Enabling Science, Technology, and Research (FREESTAR). The mission altitude was approximately 150 nautical miles with an inclination of 39 degrees. Figure 1-1 depicts the STS-107 payload bay configuration.

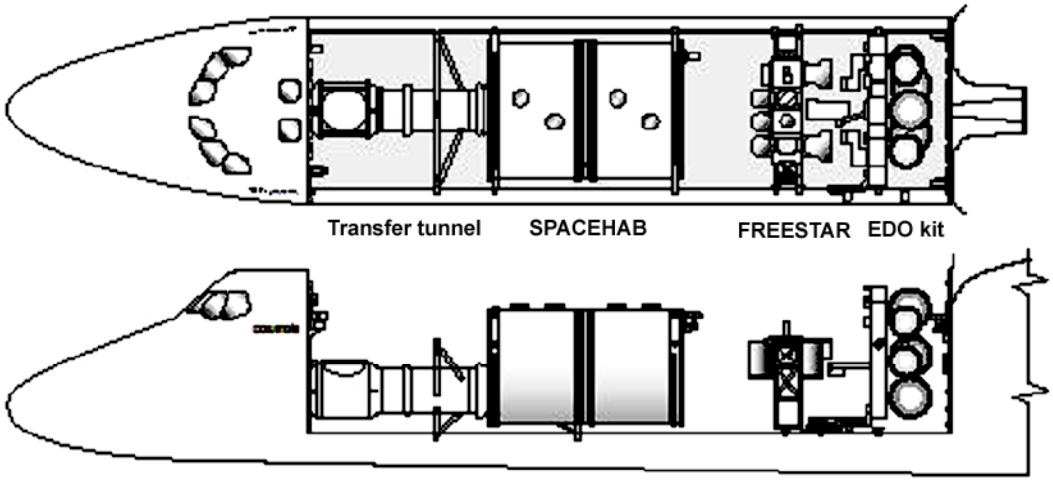

Figure 1-1. STS-107 payload bay configuration

STS-107 was a Shuttle mission dedicated to investigating human physiology, fire suppression, and other areas of research, with 80-plus experiments representing the latest application of micro gravity research. The seven-member crew devoted 16 days on-orbit to a mixed complement of research in the space, life, and physical sciences including biology, physics, and chemistry. Other investigations studied factors that control our terrestrial climate. Participants included several NASA centers, universities, and education and research organizations throughout the United States, along with the European Space Agency (ESA), the Canadian Space Agency (CSA), the Japanese National Space Development Agency (NASDA), the German Aerospace Research Establishment (DLR), and the Israeli Space Agency.

The primary payload carrier on STS-107 was the new SPACEHAB Research Double Module (RDM), doubling the volume available for, and significantly increasing the amount and complexity of, micro-gravity research. The RDM was a pressurized environment carried in Columbia's payload bay and accessible to the crew via a tunnel from the Shuttle's middeck.

SPACEHAB Inc., via commercial contracts, enabled many universities, companies, and other government agencies to conduct important research in space on STS-107. As an example, the CSA conducted three bone-growth experiments and the DLR measured the development of the gravity-sensing organs of fish in the absence of gravity's effects.

One university grew ultra-pure protein crystals for drug research while another university tested a navigation system for future satellites. The U.S. Air Force conducted communications experiments. Elementary school students in Australia, China, Israel, Japan, Liechtenstein, and the United States studied the effects of space flight on fish, spiders, ants, silkworms, bees, and even inorganic crystals.

Columbia's payload bay also housed six science payloads known as FREESTAR, which were mounted on a Multi-Purpose Experiment Support Structure bridge spanning the width of the Payload Bay (PLB). These experiments performed solar observations, earth science and atmospheric observations, fluid physics, and demonstrated new communications technology for future spacecraft. Columbia was also outfitted with an Extended Duration Orbiter (EDO) cryogenic pallet, which provided the required consumables for the long duration of the mission.

The Mediterranean Israeli Dust Experiment (MEIDEX), managed by the Israeli Space Agency and Tel-Aviv University, was one of the key FREESTAR experiments. The primary objective of MEIDEX was to observe dust storms in the Mediterranean and the Atlantic coast of Africa using a radiometric camera mounted in the payload bay, which was remotely controlled by the ground or astronauts in the crew cabin. Secondary objectives of MEIDEX included observations of slant visibility, sea-surface and desert-surface reflectivity, and Transient Luminous Events, such as sprites.

2.0 LAUNCH COUNTDOWN

The STS-107 Launch Countdown (LCD) was approximately 24 hours longer than a typical International Space Station (ISS) countdown, but within the experience base of other SPACELAB or SPACEHAB-type missions. There were some differences in this countdown as compared to most LCDs, primarily because this was not an ISS mission. Some of the more significant differences were due to the Extended Duration Orbiter (EDO) pallet that provided additional electrical power generation capability for this 16-day science mission, and the fact that the SPACEHAB module had to receive final stowage late in the countdown to accommodate the live animals and other unique science payloads. Figure 2-1 details the STS-107 LCD overview flowchart.

There were no significant issues during the LCD including the Power Reactants Storage Device (PRSD) cryogenic load or EDO planned offload operations. The crew module activities were in the critical path from L-48 hours (post-PRSD) through the start of External Tank (ET) loading due to the amount of SPACEHAB and middeck stowage items. The SPACEHAB stowage activities were completed approximately 90 minutes late due to configuration issues and the significant amount of equipment to stow. However, the LCD team was back on the critical path timeline by the completion of the communication system activation (~ L-24 hours).

ET propellant loading was delayed by approximately 70 minutes (started at L-7 hours, 20 minutes) due to several factors. These factors included the fuel cell activation/calibration running longer than planned because the time allocated for this activity was not adequate for the additional cryogenic tanks on the EDO pallet. Also, the work to resolve Interim Problem Report 110 (IPR 107V-0110), which was written to document a Liquid Oxygen (LO2) replenish valve problem, required access to the Mobile Launch Platform (MLP) and delayed preparation for ET LO2 filling operations. As a result of troubleshooting for another IPR (IPR 107V-0108, Front-End Processor (FEP) 661 Unplanned Swap), a Launch Processing System (LPS) reconfiguration of the active/standby launch data bus FEP power supplies was required to provide power redundancy for ET loading.

LO2 and LH2 tank loading were both normal, and all loading cycles were within previous experience. According to postflight analysis, at the end of propellant loading (end of replenish), the LH2 tank load was 231,035 pounds mass (lbm), and the LO2 tank load was 1,382,980 lbm. The postflight analysis includes corrections for the specific ET volume for both tanks and helium injection density corrections for the LO2 tank.

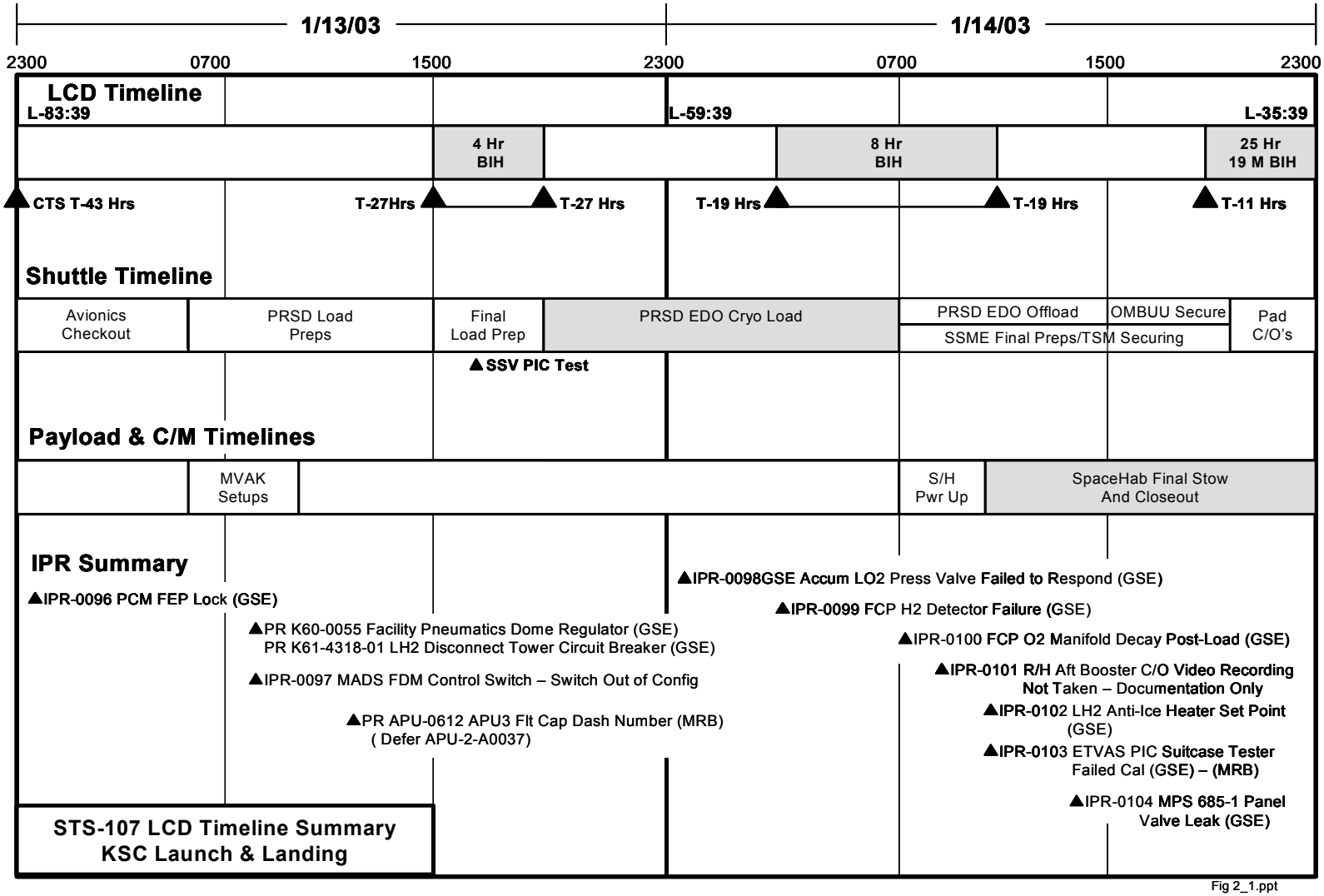

Figure 2-1. STS-107 Launch Countdown (LCD) overview flowchart

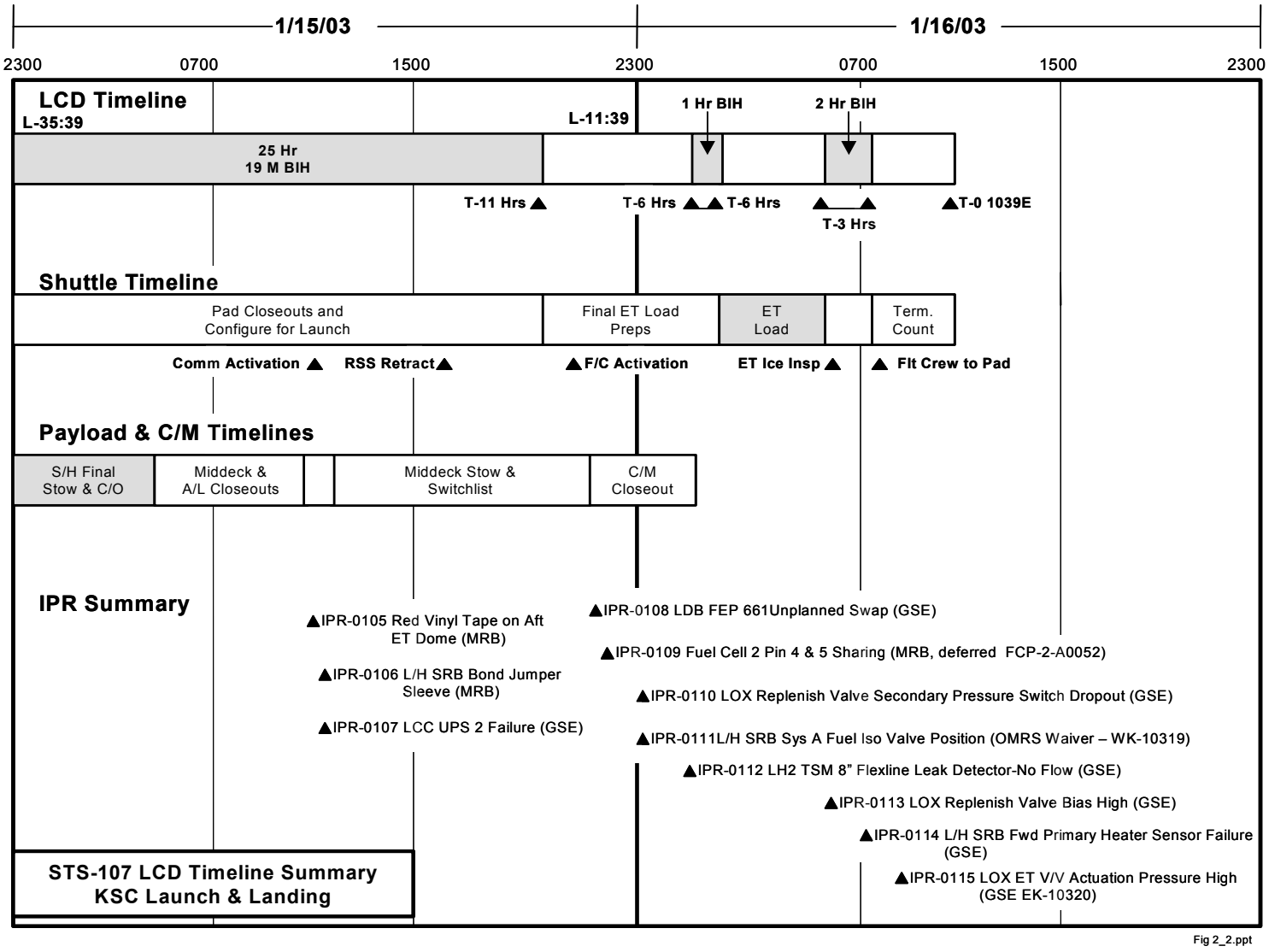

Figure 2-1. STS-107 Launch Countdown (LCD) overview flowchart (concluded)

The post-ET load Ice Team inspection was performed with no significant issues noted relative to previous inspections. The inspection began at 6:15 EST and finished at 7:45 EST. The weather conditions at the start of inspection were as follows: temperature 48 degrees Fahrenheit, relative humidity 97 percent, winds from 290 degrees at 5 knots. One item of interest was noted with respect to the -Y (left) bipod ramp closeout area (see Figure 2-2 for vehicle coordinate system orientation). The Liquid Hydrogen (LH2) section of the Ice Team report noted that there were visual indications of frost along the bondline of the ET -Y bipod, and that the frost dissipated by 7:15 EST, after sunrise. The ET bipod assembly is located at the forward ET/orbiter attach point, and indications of frost are not unusual in this area.

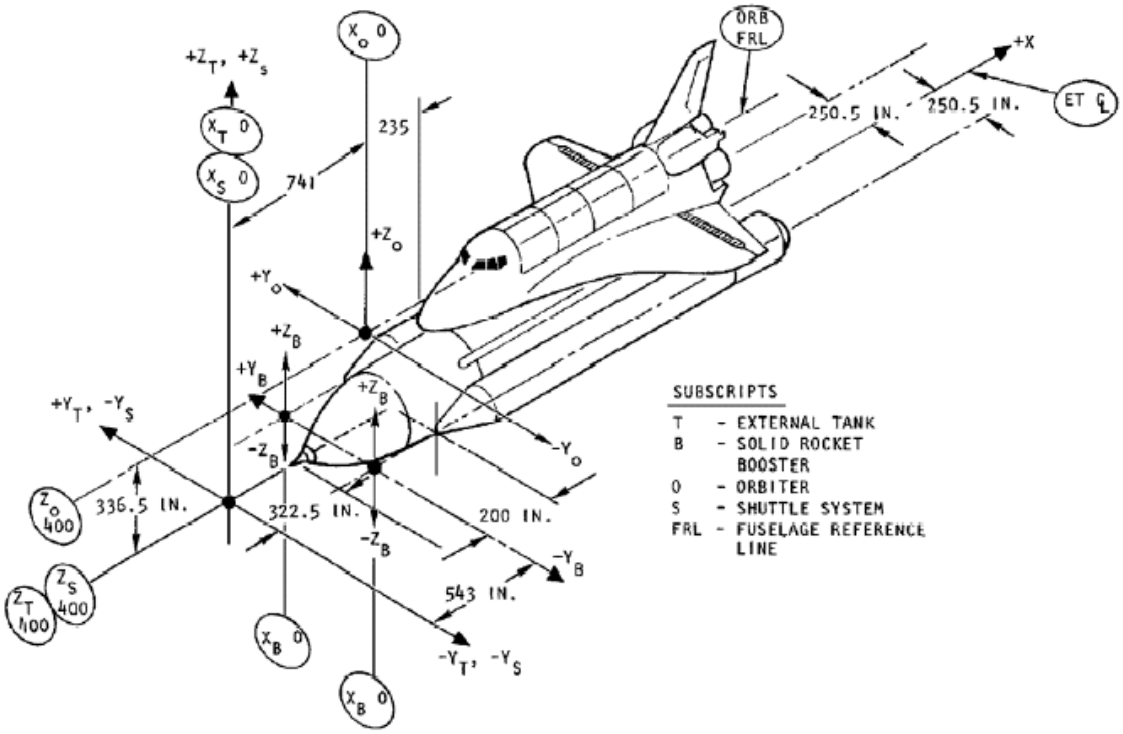

Figure 2-2. Shuttle vehicle coordinate system

The postlaunch debris walk down was performed at the launch pad per Operations and Maintenance Instruction (OMI) S6444, and no unusual debris or damage was noted. All IPRs and Problem Reports (PRs) recorded during the LCD were evaluated and three were noted as worthy of discussion since they involve possible ascent debris or the ET. The first, IPR 107V-0102, LH2 Anti-Ice Heater Failed Set Point, was written to document a Ground Support Equipment (GSE) heater that did not control to the required set point within the specified time. The Alternating Current (AC) phasing was found incorrectly wired due to a previous modification. The associated power leads were swapped and retested on the second day of the LCD without incident. This system performed nominally for the remainder of the LCD.

The second item, IPR 107V-0105, Red Vinyl Tape on Aft ET Dome, was written to document a small piece of red vinyl tape (1 in. by 1.5 in.), similar to that used in Solid Rocket Booster (SRB) closeout activity, which was found adhered to the +Y side of the ET LH2 aft dome (Y-Y axis approximately 1 ft aft of station XT2058) during the L-1 day walk down. There was no visible Thermal Protection System (TPS) damage noted in the vicinity of the tape. The tape was accepted to use as-is via the Material Review Board (MRB) process. The rationale was that the tape was limited in size and mass, presented no adverse effect to the TPS performance, and was outside of the critical debris zone since it was located on the very bottom part of the ET.

The third item was IPR 107V-0106, Booster Bond Jumper Sleeve Not Removed. This IPR was written for a part marking identification sleeve found on the systems tunnel ground strap 5 feet below the aft web of the right booster ET attach ring near the booster factory joint Xb-1577. The small plastic sleeve was accepted via Material Review (MR) board to use “as-is,” because the sleeve and strap would not be affected by aero heating, and if the sleeve melted or tore away during ascent, its trajectory would be outside the orbiter debris zone.

3.0 LAUNCH

3.1 INTRODUCTION

This section discusses the launch and ascent phases of STS-107 in four separate sections. The first section outlines some general launch conditions and an introduction to the ET bipod foam impact, including photographic and debris transport analyses, as well as RCC impact testing and analyses. The next section discusses several key MADS measurement signatures from the ET foam impact timeframe. This is followed by a summary of launch and ascent radar, and corresponding analyses. The final section is a detailed discussion of several orbiter Guidance, Navigation, and Control (GNC) system events of interest from the ascent timeframe. These include wind shear, ascent loads, ET propellant slosh, and SSME and SRB nozzle positions. The discussion centers around possible correlation of these events with other families of flights, including the family of flights where it is known that ET bipod foam loss occurred.

3.2 LAUNCH DEBRIS IMPACT OBSERVATION

3.2.1 Launch/Ascent Conditions

Launch occurred at the Kennedy Space Center (KSC), launch pad 39A, on January 16, 2003, at 10:39 EST (see Figure 3-1). The weather at pad 39A, 60-foot level was: temperature 65 degrees Fahrenheit, relative humidity 68 percent, dew point 59 degrees Fahrenheit, with calm winds. Figure 3-2 shows the STS-107 reconstructed altitude data and Figure 3-3 shows the mach number and dynamic pressure during first stage, prior to Solid Rocket Booster (SRB) separation, as a function of Mission Elapsed Time (MET).

Figure 3-1. Launch of STS-107 at pad 39A at Kennedy Space Center

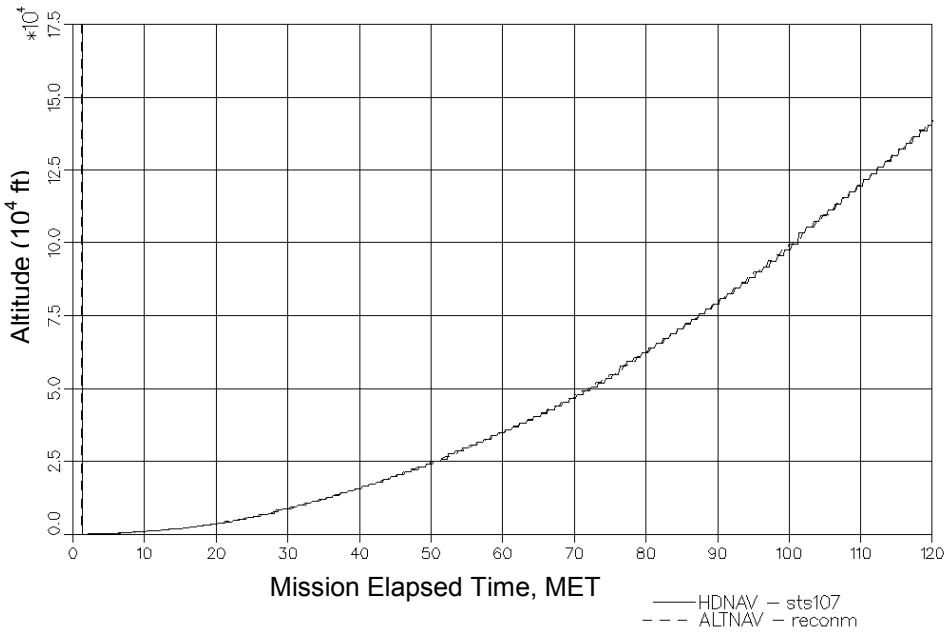

Figure 3-2. STS-107 reconstructed altitude during first stage (prior to SRB separation)

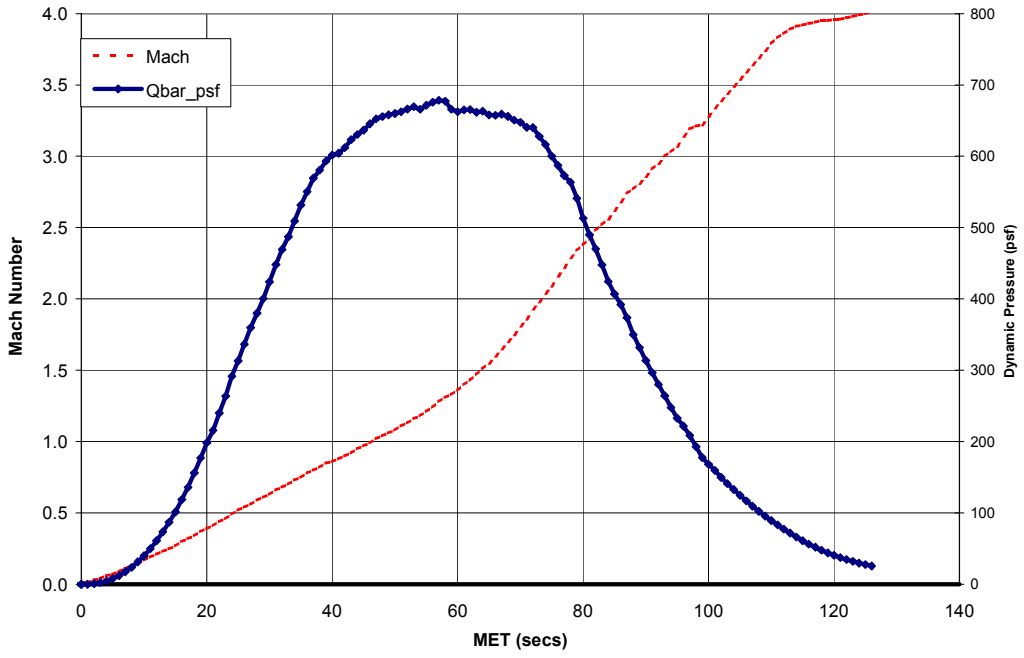

Figure 3-3. STS-107 flight reconstruction data for mach number and dynamic pressure (Q-bar) prior to SRB separation. Note that Q-bar is highest during first stage (prior to SRB separation), and reduces to a very small number after SRB separation

3.2.2 Launch Debris Impact Area

Postlaunch photographic analysis determined that one major piece of foam and at least two minor pieces departed the External Tank (ET) left bipod ramp area approximately 82 seconds after launch. The primary foam piece impacted Columbia in the vicinity of the lower left wing Reinforced Carbon-Carbon (RCC) panels 5 through 9 at 81.86 seconds after launch. There were no indications that any of the minor pieces impacted the left wing based on their post-separation trajectories. The orbiter was at an altitude of ~65,860 feet, traveling at Mach 2.46 at time of impact.

Several approaches were taken to assess the area of left wing damage. The efforts included launch video and photograph analysis, review of launch MADS data, debris transport analysis, forensic analysis of debris found in Texas, wire bundle burn through analysis, and aero/thermal modeling of the entry. The data indicate that the area of the highest probability of damage to the left wing was between RCC panels 5 and 9, with the most likely damage occurring on the lower side of RCC panel 8 or an adjacent Tee seal. The damage was most likely equivalent in size to a 6 to 10 inch diameter hole or area broken from the RCC panel or an adjacent Tee seal. Figure 3-4 shows the area of highest probability of wing damage and Table 3-1 shows the methods used to determine the damage.

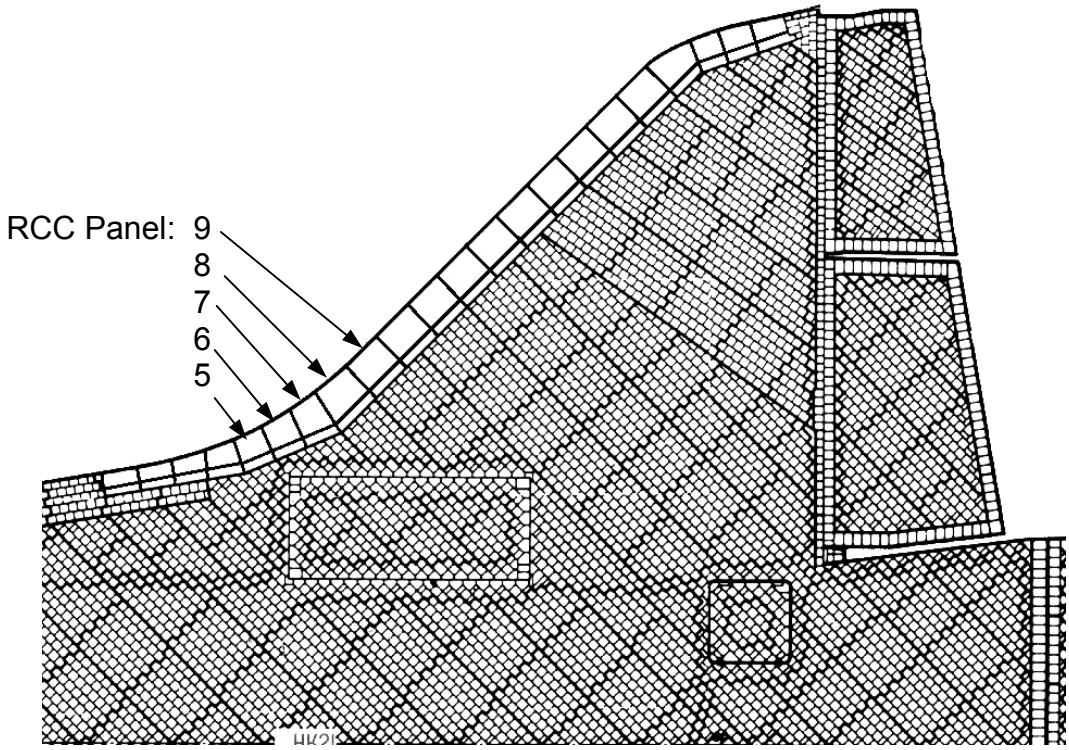

Figure 3-4. Area of most likely wing damage

Table 3-1. Wing damage analysis methods and results

WING DAMAGE ANALYSIS METHOD	PREDICTED DAMAGE AREA	COMMENTS	DISCUSSION FOUND IN SECTION
LAUNCH VIDEO AND PHOTO ANALYSIS	RCC 5 through 9	Most likely area of impact was RCC panels 6 through 8.	3.2
ASCENT MADS DATA	RCC 6 through 8	Unusual temperature sensor data observed on spar behind RCC panel 9, and temperature rise matches a thermal math model of a 10 inch diameter hole in RCC panel 8.	3.3
DEBRIS TRANSPORT ANALYSIS	RCC 5 through 8	Most likely area of impact was RCC panels 6 through 8.	3.2
HARDWARE FORENSICS DATA	RCC 8 or 9	Fragments of RCC panels 8 and 9 showed extreme temperature indications, knife edge heat erosion patterns, and heavy amounts of slag deposited on the insides of those panels.	5.3
ENTRY MADS DATA	RCC 8 or 9	First unusual indication observed during entry was a strain gauge behind RCC panel 9 (could be due to a strain behind adjacent panel 8).	5.4
WIRE BUNDLE BURN THROUGH	RCC 7 through 9	Burn through from locations forward of panel 7 or aft of panel 9 are very unlikely based on sensor data loss timing.	5.4
ENTRY AERO/THERMAL MODELING	RCC 8 or 9	Based on wind tunnel test results and CFD analysis.	5.5

3.2.3 Launch Photo and Transport Analysis

Photographic analysis of the debris impact event included participation from the Johnson Space Center, the Marshall Space Flight Center, the Kennedy Space Center, Lockheed Martin Management and Data Systems, Boeing NASA Systems, the Eastman Kodak Company, and the National Imaging and Mapping Agency.

Video and Computer-Aided Design (CAD) analysis determined that the most likely impact location was leading edge RCC panels 6 through 8 (Figure 3-5). Due to the foam size, RCC panels 5 and 9 must also be included in this impact zone. The best estimate of the foam size, based on imagery measurements, is 21 to 27 inches long and 12 to 18 inches wide. The precise foam shape and thickness cannot be determined from the available imagery; however, a reasonable estimate is that it was a plate-like shape and several inches thick. The foam tumbled at a minimum rate of 18 times per second based on the imagery, although the actual rate may never be known more accurately. Figure 3-6 illustrates a portion of the photographic analysis techniques used to determine the size of the foam.

The most useful video analysis was performed using two cameras that are part of the Eastern Launch Range imaging system. Camera E212 (film), located on the Cape Canaveral Air Force Station, was approximately 17 miles from the orbiter at the time of foam impact and Camera ET208 (video), located in Cocoa Beach, Florida, was 26 miles from the orbiter. The overall camera geometry relative to the launch pad and ascent flight path is shown in Figure 3-7. Camera E212 had a better view of the topside of the launch vehicle, while Camera ET208 had a better bottom side view. Figure 3-8 depicts the view from each of the camera systems. A third camera, E208 (film), also recorded the launch but was blurred and contained no useful data for the investigation. There are no Launch Commit Criteria (LCC) regarding cameras, or camera views for ascent, for either onboard or ground.

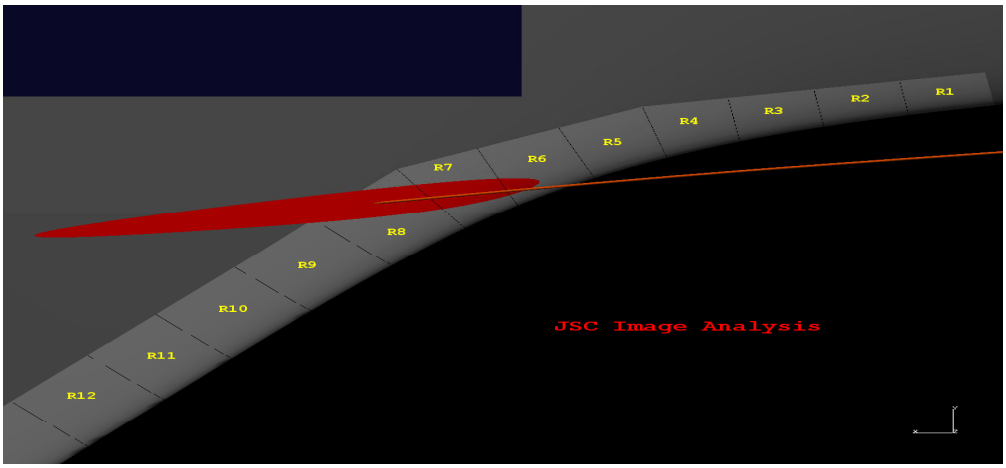

Figure 3-5. Multiple analyses determine foam impacted lower RCC panels 6 through 8 area

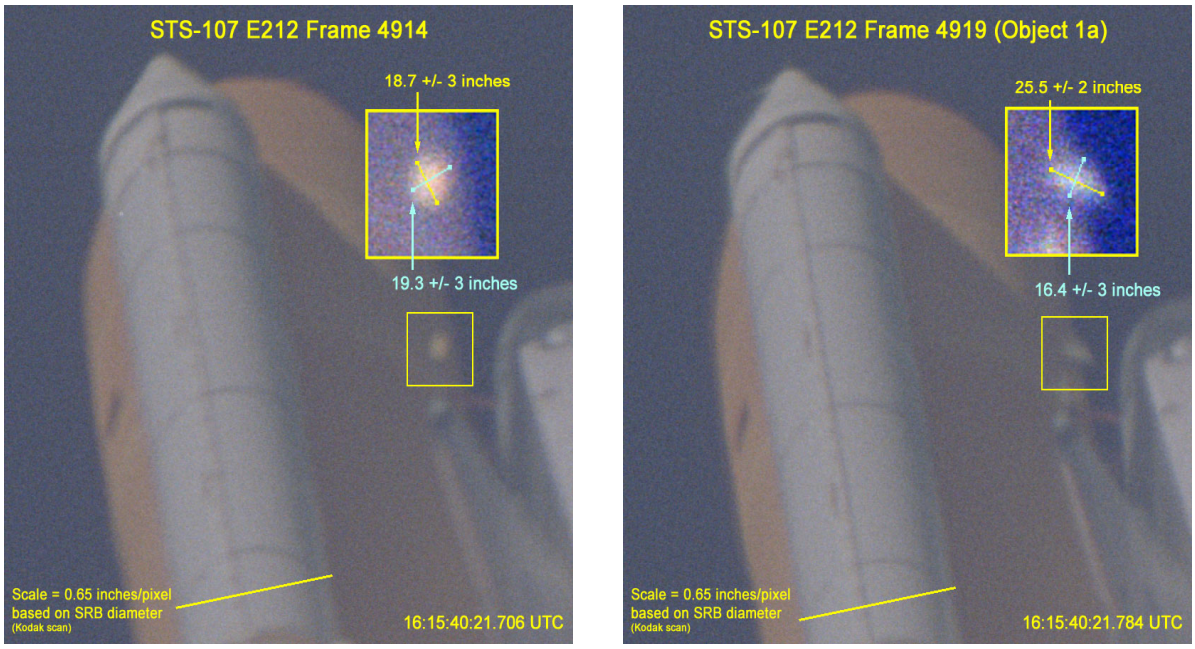

Figure 3-6. Photographic analysis techniques determined foam size: debris appears almost circular in frame 4914 and elongated in frame 4919

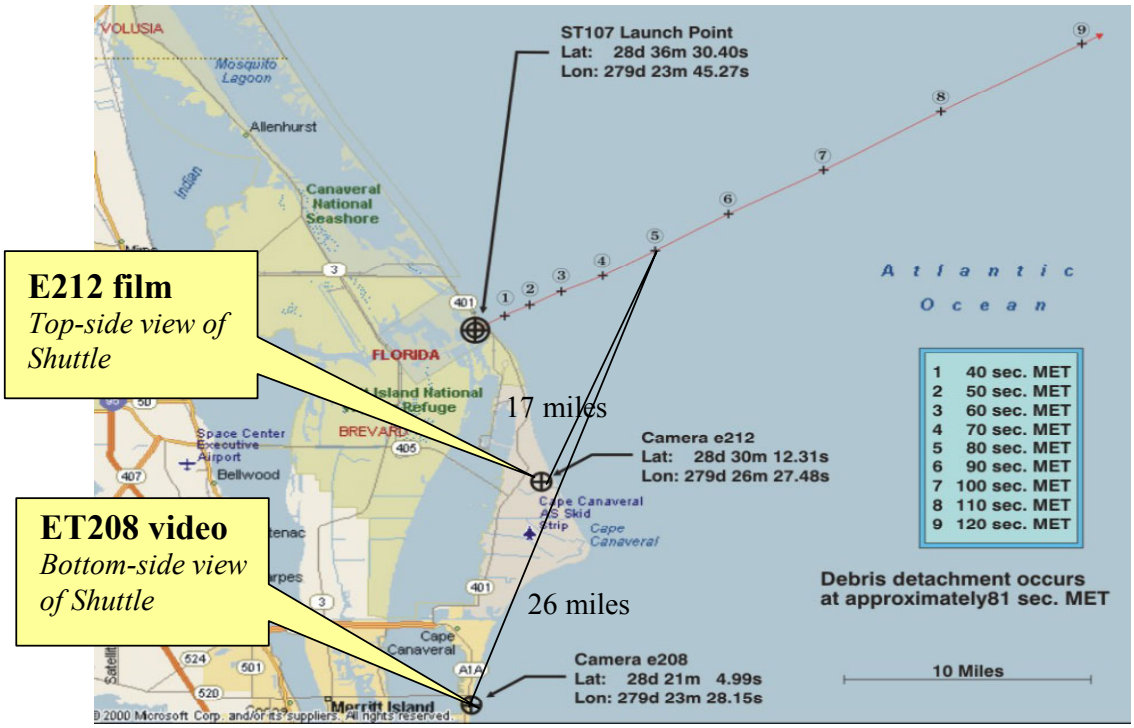

Figure 3-7. Camera geometry for ascent video analysis; note that video camera ET208 is at same location as film camera E208

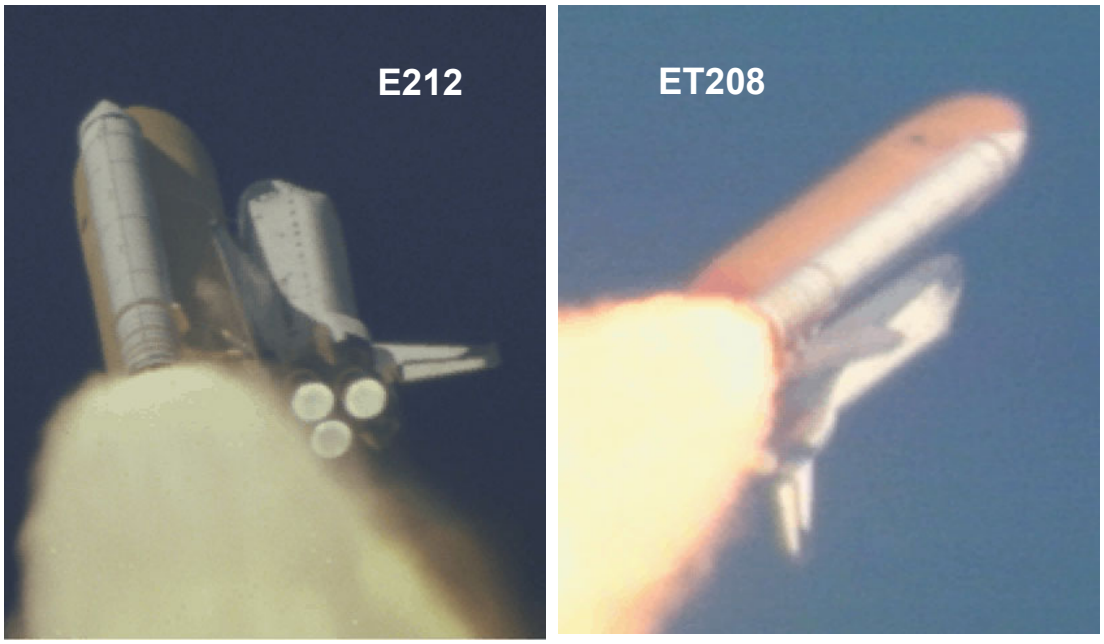

Figure 3-8. Orbiter view from Cameras E212 and ET208

There is significant visual and debris trajectory information to implicate the left bipod ramp area as the source of debris. In Figure 3-9, the red line depicts the estimated foam trajectory as it moved from the bipod ramp area toward the left wing. In addition to locating the impact in the RCC panels 6 through 8 region, the video analysis has also shown that the impact was below the apex of the RCC panels since no foam or post impact debris was observed to traverse over the top of the wing. This is indicative of an impact below the wing leading edge aerodynamic stagnation line (Figure 3-10). The stagnation line, or dividing streamline, is the line along the leading edge of the wing where the airflow comes to rest; above this line, airflow moves over the upper wing surface and below this line, the airflow moves over the lower wing surface.

Enhancements of the ascent video indicated there was no discernable damage to the orbiter wing leading edge or lower tile surface. Figure 3-11 is a sample of these video enhancements. The figure compares 30 pre-impact integrated video fields with 21 post-impact integrated video fields. Based on these enhancements, photo experts have been unable to determine or quantify any damage to any portion of the orbiter vehicle as a result of the impact.

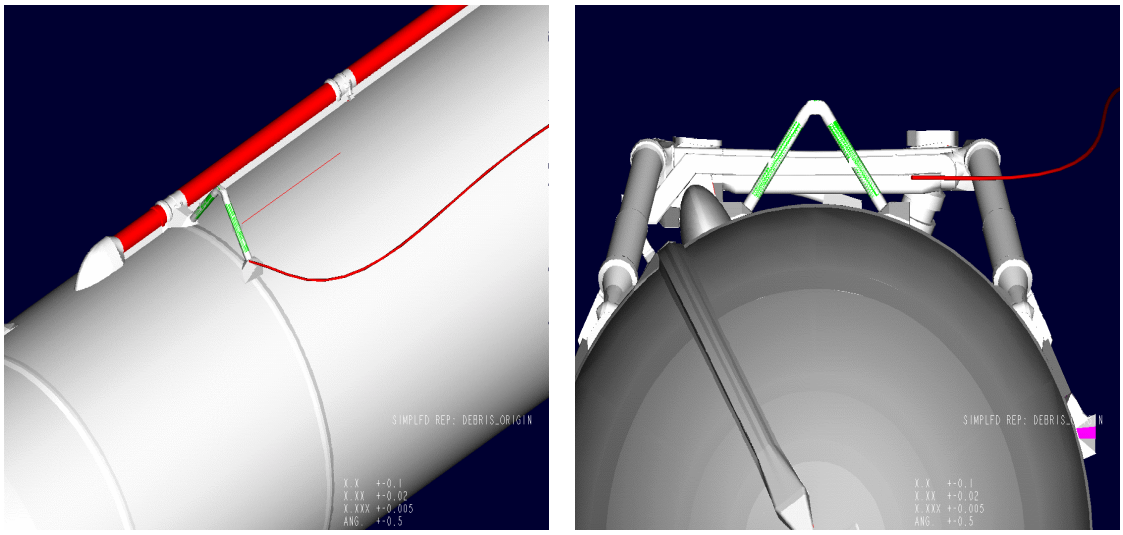

Figure 3-9. Multiple analyses indicate foam is from ET left bipod area. Red line depicts the estimated foam trajectory as it moved from the bipod ramp area toward the left wing.

Figure 3-10. Video analysis shows impact is below wing leading edge stagnation line. Trajectories of particles are depicted after the impact.

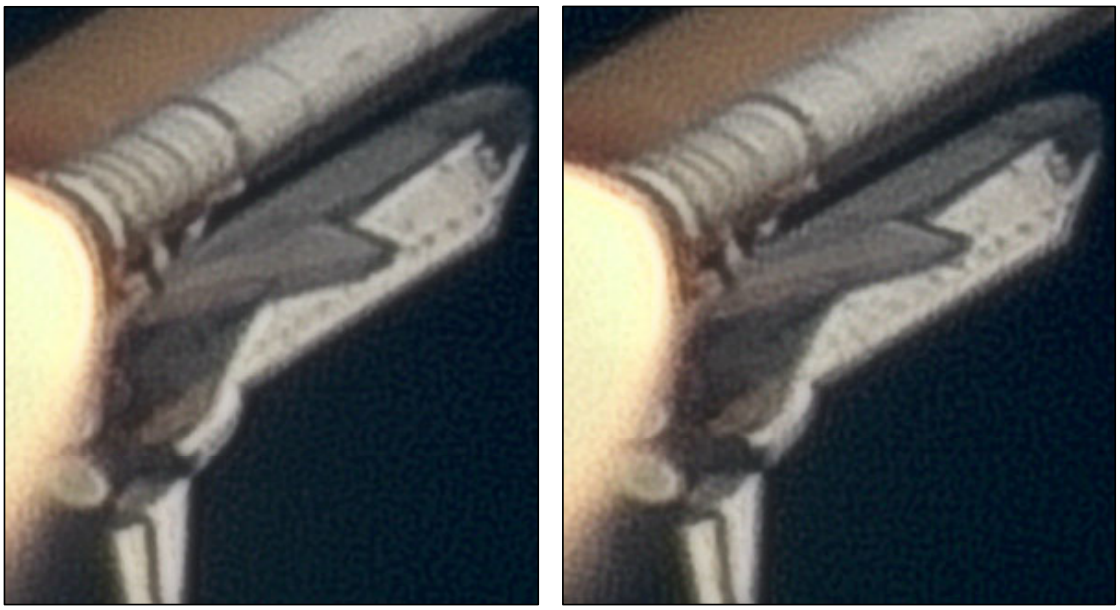

Figure 3-11. Pre-impact vs. post-impact shows no observable damage within the resolution limits

3.2.4 Debris Velocity and Size Assessment

In addition to size and location of the foam impact, there are several other parameters necessary to complete the postflight analysis of possible impact damage. These include an estimate of the foam's mass, relative velocity at impact, rotational energy, and the angle of impact with respect to the Shuttle wing at the point of impact. These parameters combine to determine the amount of impulse imparted at impact and are therefore critical to determine whether there was possible damage to the RCC panel, associated attach fitting hardware, or other leading edge structure.

Photographic analysis was used to establish a range of relative impact velocities, from 625 to 840 feet per second (416 to 573 miles per hour). This large uncertainty is due to the small number of video and film frames between release of the foam and impact with the wing, since the estimated time between the foam release and foam impact is only 0.2 seconds. The predominant direction of motion is toward the aft of the orbiter along the X-axis, although the foam is moving slightly outboard at the time of impact with little to no motion in the Z-axis (see Figure 2-2 for vehicle coordinate system orientation). The direction of motion is from the ET bipod area toward the left wing at an angle of 2 to 10 degrees with respect to the orbiter X-axis in the orbiter X-Y plane. The motion is slightly toward the wing surface at a 0 to 3 degree angle measured in the orbiter X-Z plane.

Three-dimensional trajectories from the launch films and videos were refined using a physics-based trajectory fit that included a realistic flow field model generated using computational fluid dynamics (CFD) techniques. These results indicated that the relative velocity at impact was in the range of 775 to 820 feet per second. The CFD analysis used numerical methods to model the flow field around the orbiter/ET/Solid

Rocket Booster (SRB) stack including the SRB and Space Shuttle Main Engine (SSME) plumes. An example of this analysis is shown in Figure 3-12.

The transport analysis was also used to estimate a range of sizes and corresponding weights for the foam, which are summarized in Table 3-2. For an impact velocity of 820 feet per second, the estimated foam volume is approximately 1025 cubic inches with a weight of 1.42 pounds assuming the density of the foam was 2.4 pounds per cubic foot. Similarly, for a velocity of 775 feet per second, the estimated volume is 1240 cubic inches, and the resulting weight is 1.72 pounds. Additional results produced with a more complex CFD model included lift forces and the unsteady rotation of the debris. Table 3-2 also lists the ET Working Group estimate of the bipod foam size and weight. This estimate was for one particular ET bipod ramp configuration and did not account for manufacturing variability. Thus, it was not used as the volume for the RCC impact testing, and more details are included in Section 11.

Numerous factors could affect mass of the foam debris, and the exact volume and mass may never be known. For example, the BX-250 foam could have had a higher than predicted density of 2.4 pounds per cubic foot, since the density can range from 1.8 to 2.6 lb/ft^3. Alternatively, a lower drag coefficient on the debris could also account for a higher ballistic number (BN).

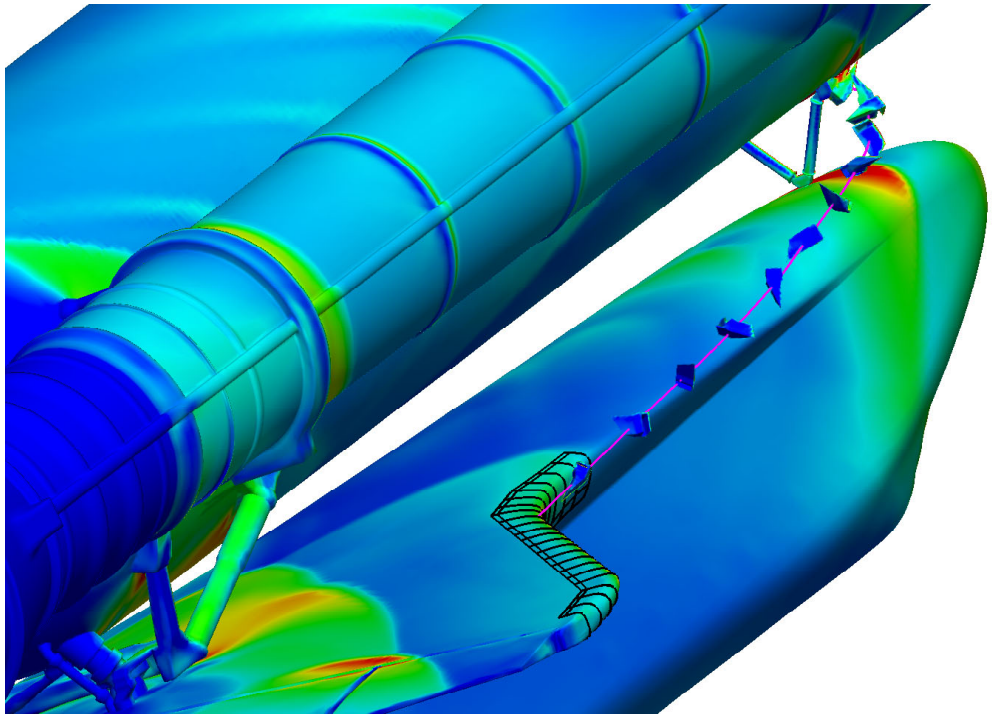

Figure 3-12. Sample CFD flow field with debris modeling

Table 3-2. Transport analysis and ET Working Group estimates of ET bipod debris size, weight, and volume

	Transport Analysis Lower Bound	Transport Analysis Upper Bound	ET Working Group Estimate	RCC Impact Testing Target
Ballistic Number (BN)	1.2	1.45	1.0	1.45
Velocity (ft/sec)	820	775	850	775
Volume (in^3) @ 2.4 lb/ft^3	1025	1240	855	1200
Weight (lbs) @ 2.4 lb/ft^3	1.42	1.72	1.19	1.67

3.2.5 Impact Damage Testing and Analysis

Analysis and experimental results were used to assess the potential for debris impact to damage Columbia's wing leading edge. The overall concept was to replicate, to the greatest extent feasible, the debris impact event that occurred on Columbia's left wing during ascent, by impacting flight-ready composite panel assemblies with a representative foam projectile fired from a compressed gas gun. The target panel assemblies had a flight history similar to that of Columbia, and were mounted on a support structurally equivalent to Columbia's left wing. The attaching hardware and fittings were either flight certified, or built to Columbia's drawings. BX-250 foam, without entrained ablator material, was used for the impacting projectile material because it represented the ascent event and provided a lower bound damage assessment. After significant study and consideration of all inputs by the NAIT and CAIB members, the parameters for representative impacts were established as: foam volume 1200 cubic inches, velocity 775 feet per second, and foam mass 1.67 pounds.

Impact testing has been completed on full size fiberglass panels, an RCC panel 6, and an RCC panel 8 to obtain insight and experimental data important to the understanding and modeling of the response of the wing leading edge components. The RCC panel 6 assembly was from Discovery and had flown 30 missions, and the RCC panel 8 was from Atlantis and had flown 27 previous missions.

The test of the RCC composite panel assembly 6 demonstrated that a foam impact representative of the debris strike at 82 seconds was capable of damaging RCC material. A 5.5 inch crack was created, extending from a visible 3/4 inch diameter damage area on the outside of the panel to the rib inside the wing. The panel 6/7 Tee seal was also damaged with a 2.5-inch crack, and the Tee seal as well as panel 6 were shifted in position. In addition, a carrier panel on the upper side of the wing was chipped.

Subsequent engineering testing has demonstrated that the localized impact loads imposed on the panel 6 assembly would have been substantially higher with changes in foam impact orientation and location. These changes were included in the RCC panel 8 assembly test and included a 30 degree clocking angle (orientation of the foam projectile relative to the target), a 22 degree angle relative to the impact surface, and an impact location lower and farther outboard relative to the panel 6 test. Impact target location was six inches farther down the trajectory track from the earlier tests. The test generated a 16 inch by 16 inch hole in the lower surface of panel 8, which is the most substantial damage to date in any RCC impact test.

The exact flight damage is unknown but is believed to be bracketed by these two tests. The testing is important in that it confirms that the ET bipod foam can catastrophically damage the RCC.

3.3 LAUNCH MADS DATA

There are two other indications that the foam impact occurred in the panels 6 through 8 area. Two Modular Auxiliary Data System (MADS) lower surface pressure measurements behaved anomalously immediately after the time of the impact. Figure 3-13 shows the location of these measurements along with possible areas for post-impact debris re-contact in the vicinity of the sensors. The unusual behavior of one of the sensors is shown in Figure 3-14.

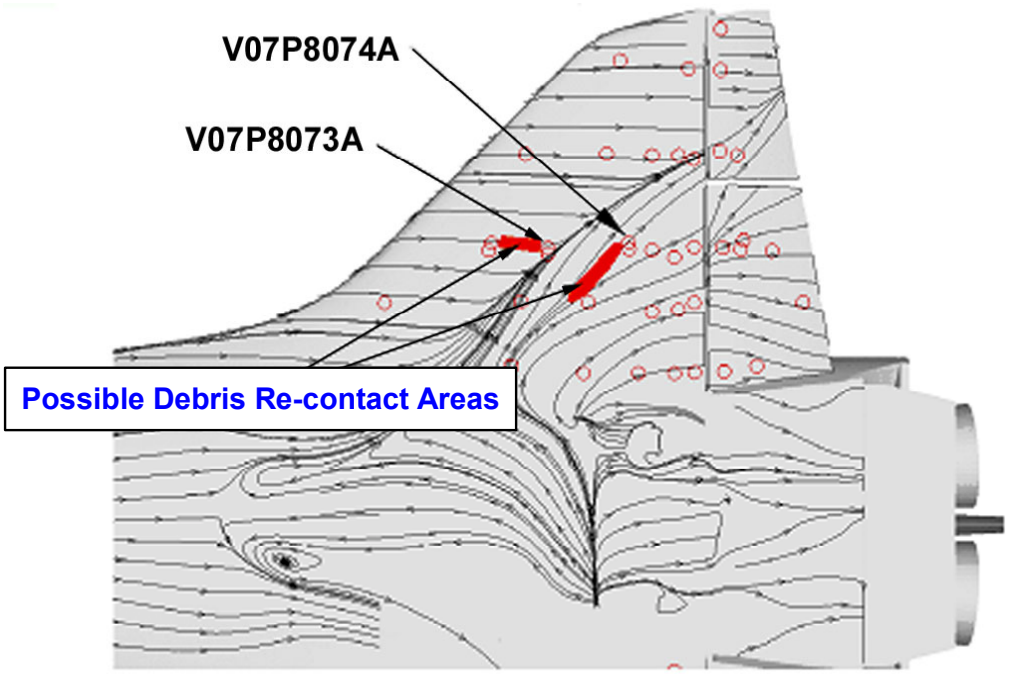

Figure 3-13. CFD surface flow with lower left wing pressure sensors

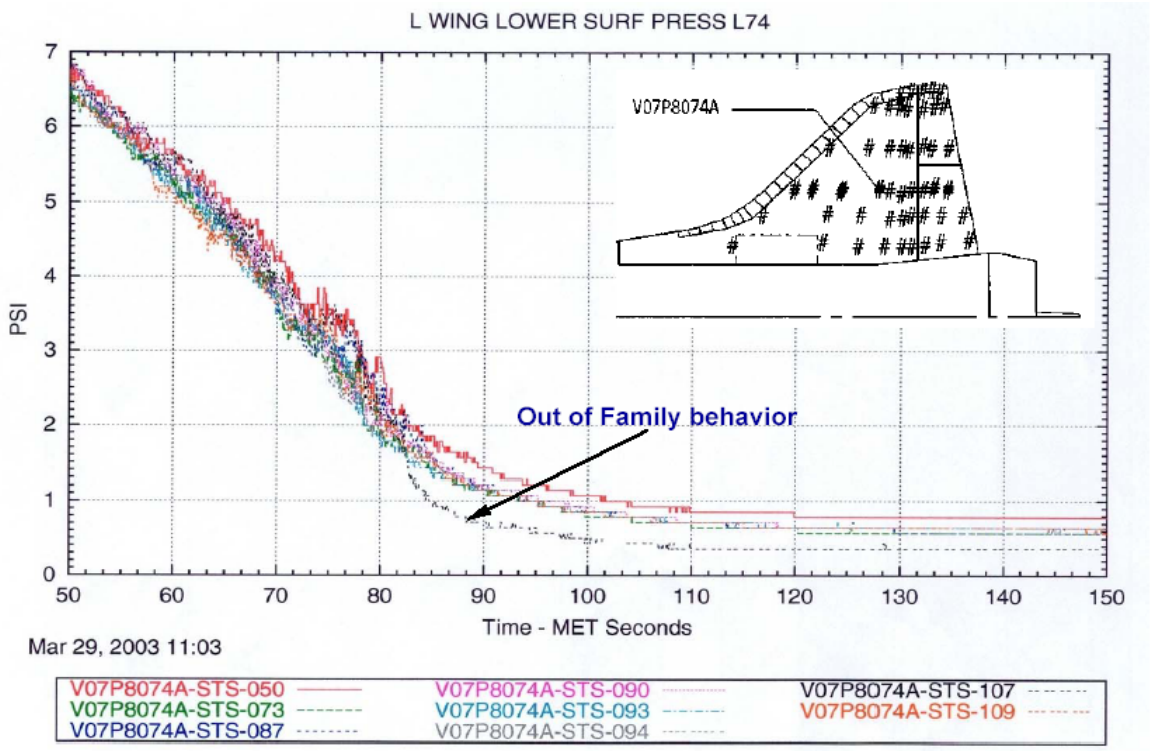

Figure 3-14. Unusual behavior of pressure sensor V07P8074A

Additionally, there is another MADS measurement that had an off-nominal signature during the ascent timeframe. The temperature sensor on the leading edge spar behind RCC panel 9 showed a slightly higher temperature rise than seen on any previous Columbia flight. Figure 3-15 shows the location of the temperature sensor behind the wing leading edge spar inside the wing. The slight temperature rise can be seen in Figure 3-16. Note that most flights show a small rise in this temperature during ascent due to aerodynamic heating.

STS-107 had a 7.5 degree Fahrenheit rise that started very early during ascent (five to six minutes after launch). Although the data do not prove that the RCC was breached during ascent, the data are consistent with a possible flow path into the RCC cavity via damage in the RCC panels 6 through 8 area. A simplified thermal math model was constructed and verified with flight data from STS-5. The model was then correlated to the flight data from STS-107. Assuming the equivalent heating from a 10 inch diameter hole in RCC panel 8, this model nearly predicts both the ascent and entry temperature profiles for the wing leading edge spar temperature sensor. Figure 3-17 compares the model with the flight data for both ascent and entry. For comparison, Figure 3-18 shows the overall heating rate of the STS-107 ascent and entry environments on RCC panel 9. As shown, the heating on the wing leading edge is much greater during the entry profile than during the ascent profile.

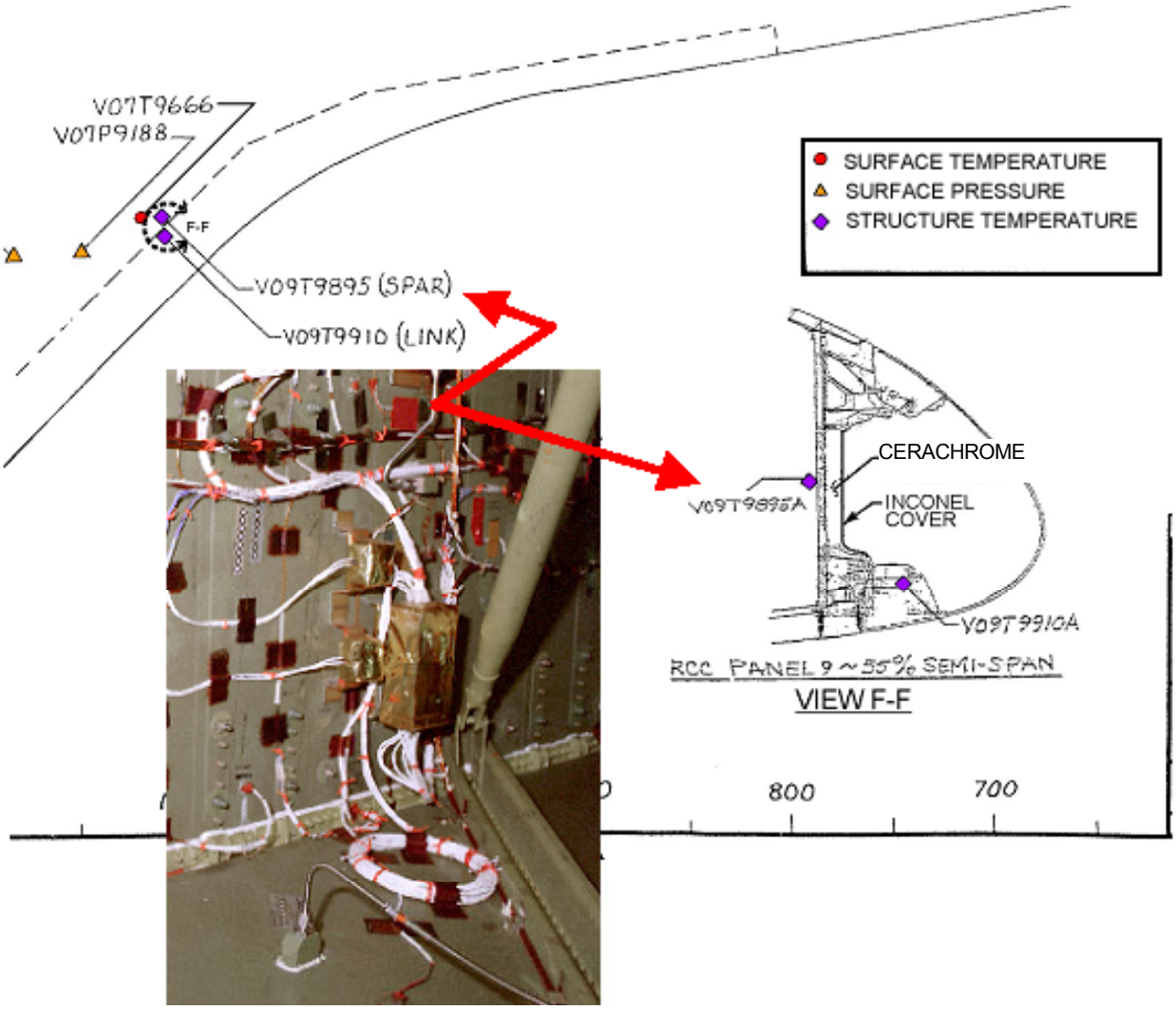

Figure 3-15. Close-out photo shows RCC panel 9 wing leading edge temperature measurement

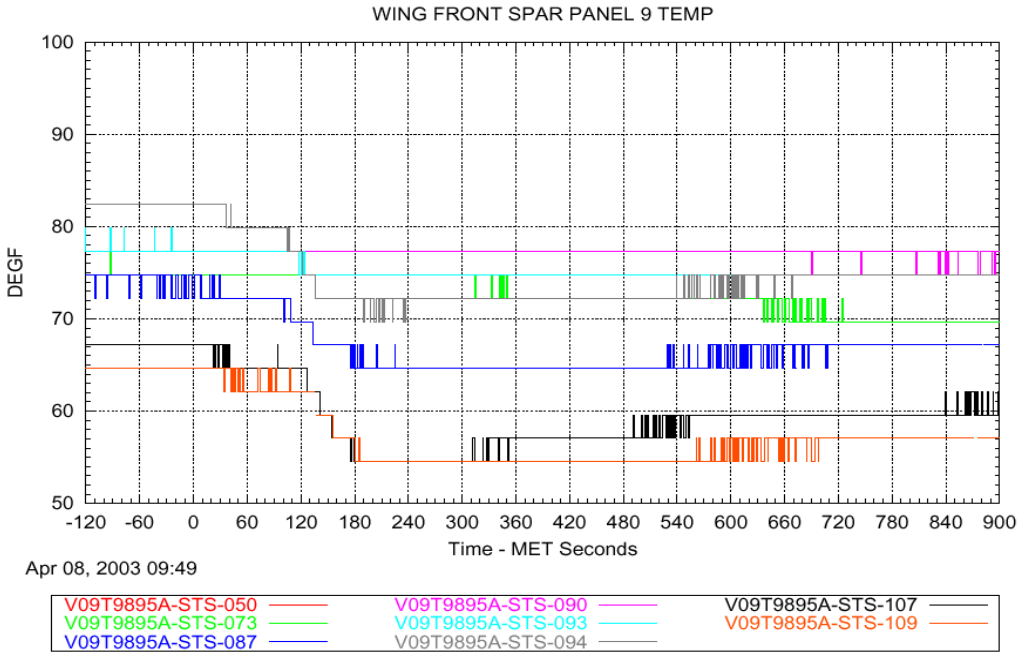

Figure 3-16. Three-bit rise (7.5 degrees F) on MADS wing leading edge spar temperature measurement (V09T9895A) during ascent

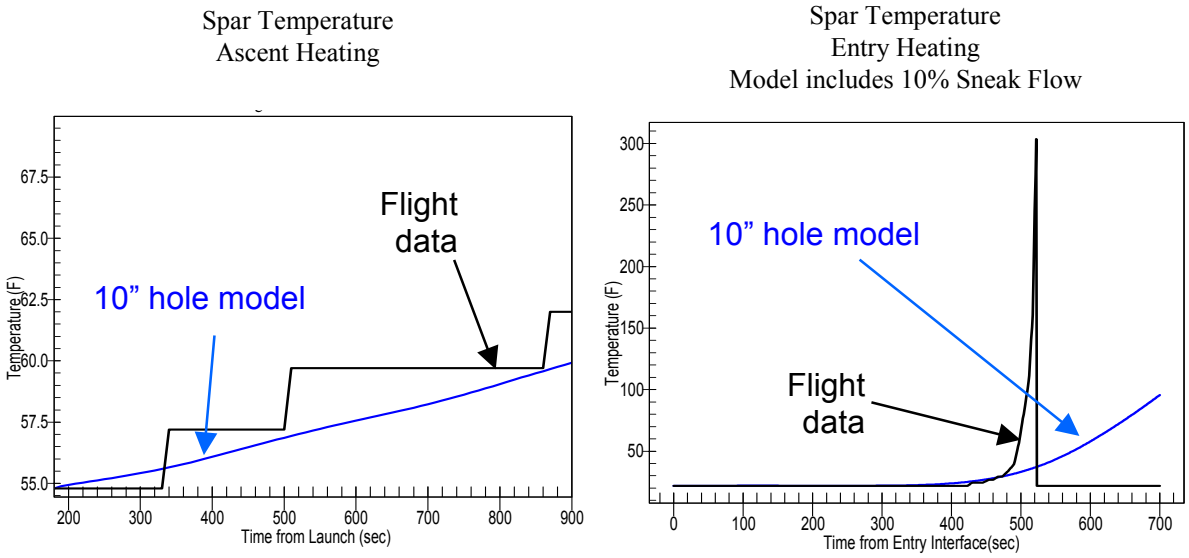

Figure 3-17. Correlation between simplified thermal math model and STS-107 ascent and entry flight data

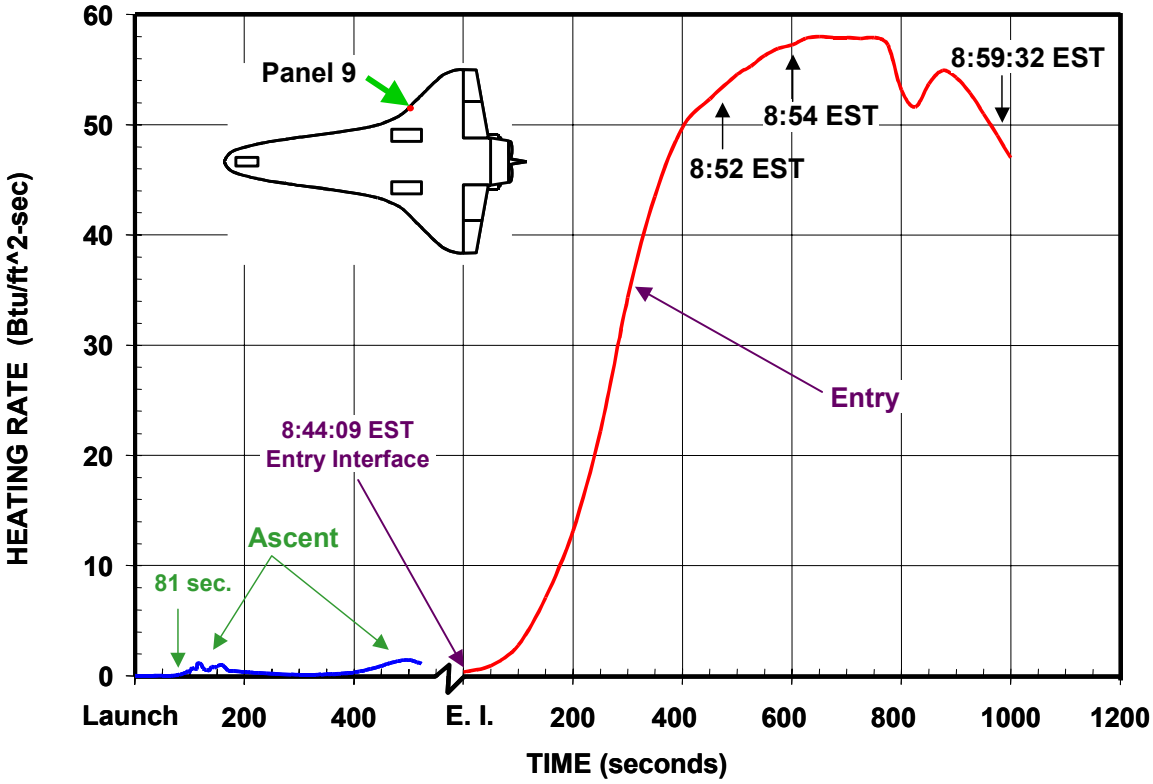

Figure 3-18. STS-107 ascent and entry heating environments on RCC panel 9

3.4 LAUNCH AREA RADAR ANALYSIS

STS-107 was tracked during ascent by the Eastern Range (ER) land-based C-Band radars, and identified debris was analyzed for time of separation, radar cross section (RCS), and range separation rate. In summary, the radars were unable to detect debris prior to SRB separation. Following SRB separation, from Launch + 150 to L + 230 seconds (2:30 to 3:50 Mission Elapsed Time, MET), 46 items were catalogued, of which 27 items are considered to be debris; however, the radar return signal was not of sufficient strength to determine the approximate shape, size, or rigidity of the debris. The radar analysis results are consistent with the debris analyses from previous STS missions. Table 3-3 lists the STS-107 catalogued radar detected events.

The launch radar is optimized for range safety and vehicle trajectory determination, and not for small debris assessment. A better radar for small debris, the Multiple-Object Tracking Radar (MOTR) was not available for use on STS-107. The ER radars used on STS-107 were not designed for signature analysis and were not able to lock onto and track multiple targets simultaneously. Additionally, debris could remain undetected if the debris was emitted at a time and angle where it was shielded from the radar by the vehicle body.

Detailed postlaunch radar debris analysis was performed on a regular basis until STS-57. There are reports available from previous flights, and typical observations include low strength radar returns from SRB separation to T + 300 seconds.

In general, the strength of the radar (C-band, AN/FPQ-14 unit) return depends on distance to the object, size of the object, and reflectivity of the object. For the STS-107 analyses, the distance to the objects is known but the object size and reflectivity are unknowns for all objects detected. As such, it was necessary to perform an exclusionary exercise to try to identify the objects. Some basic rules could be applied, such as knowledge that objects with very high separation speed are known to be part of the exhaust plume or products (such as SRB slag). In Table 3-3, items 30 and 31 were determined to be SRB slag. Moderate separation speed indicates solid objects being left behind. Separation rates can also be used to infer the density. There are limits to the debris size and shape that can be detected by the radar (see Figure 3-19 and Figure 3-20).

Table 3-3. STS-107 ascent radar events

Catalog number	Radar source (site no.)[a]	First / last appearance (T + sec)	MAX RCS[b] (dBsm)[c]	Separation rate (m/sec)	Lower RSR[d] (m/sec)	Upper RSR[d] (m/sec)
1 [e]	0.14	80.4/87	8	14	44	541
29 [e]	19.14	81.6/86.1	-1	30	36	688
34	19.14	117/121	-15	771	10	1268
30 [f]	0.14	117.5/118	-8	1240	0	1162
31 [f]	28.14	117/118.5	-11	1500	3	616
32	28.14	118/119	-8	350	0	622
35	19.14	121/122	-16	771	4	1286
36	19.14	121/125	-16	372	6	1289
37	19.14	121/123	-15	426	4	1286
38	19.14	123/126	-14	424	1	1294
39	19.14	124/126	-14	480	3	1297
40	19.14	126/127	-12	490	2	1303
41	19.14	126.5/128	-13	490	2	1306
42	19.14	127/128	-14	476	2	1307
43	19.14	128/129	-13	570	0	1310
33	28.14	128/130	1	520	1	710
44	19.14	129.5/131.5	-14	670	2	1320
45	19.14	130/132.5	-15	371	4	1324
46	19.14	130.5/131.5	-13	370	2	1320
23	28.14	152/158.5	-12	187	13	947
2	0.14	152.5/156	-10	210	9	1405
3	0.14	152.5/162.5	-8	326	26	1405
4	0.14	153/160	-9	229	104	1505
24	28.14	154.5/162	-14	400	15	975
5	0.14	156/170	-16	217	38	1465
6	0.14	158.5/171	-17	309	34	1477
7	0.14	164/170	-17	312	17	1493
8	0.14	166.5/173	-21	357	19	1513

Table 3-3. STS-107 ascent radar events (concluded)

Catalog number	Radar source (site no.)[a]	First / last appearance (T + sec)	MAX RCS[b] (dBsm)[c]	Separation rate (m/sec)	Lower RSR[d] (m/sec)	Upper RSR[d] (m/sec)
25	28.14	167/176.5	-18	221	22	1106
9	0.14	167/184.5	-15	260	53	1557
10	0.14	170/184.5	-15	265	44	1568
11	0.14	174.5/180	-14	290	17	1568
12	0.14	173/180	-16	206	21	1562
13	0.14	174/175.1	-16	244	2	1546
14	0.14	175.5/180	-15	180	14	1572
15	0.14	178/180	-14	296	8	1583
26	28.14	179/187.5	-10	884	22	1221
16	0.14	184/190	-14	236	19	1643
17	0.14	187/192.7	-11	649	19	1665
27 [g]	28.14	201/207	Low signal	Low signal	18	1438
28 [g]	28.14	205/208.5	Low signal	Low signal	11	1468
18 [g]	0.14	204.5/210	Low signal	Low signal	20	1812
19	0.14	204.5/214	-18	326	36	1829
20	0.14	204.5/212	-17	166	28	1820
21	0.14	206/212	-18	225	22	1827
22	0.14	211.5/228	-17	219	66	1926

a - Radar source: 0.14 = Patrick Air Force Base (PAFB), 19.14 = Kennedy Space Center (KSC), 28.14 = Jonathan Dickinson Missile Tracking Annex (JDMTA)

b - Radar cross section (RCS)

c - Decibels relative to one square meter (dBsm)

d - range separation rate (RSR)

e - Objects 1 and 29 are explained as plume artifacts evident by low separation rates from vehicle

f - Objects 30 and 31 are probably SRB slag ejection evident by high separation rates from vehicle

g - Objects 27, 28, and 18 had indeterminable RCS and RSR due to low level of signal returns

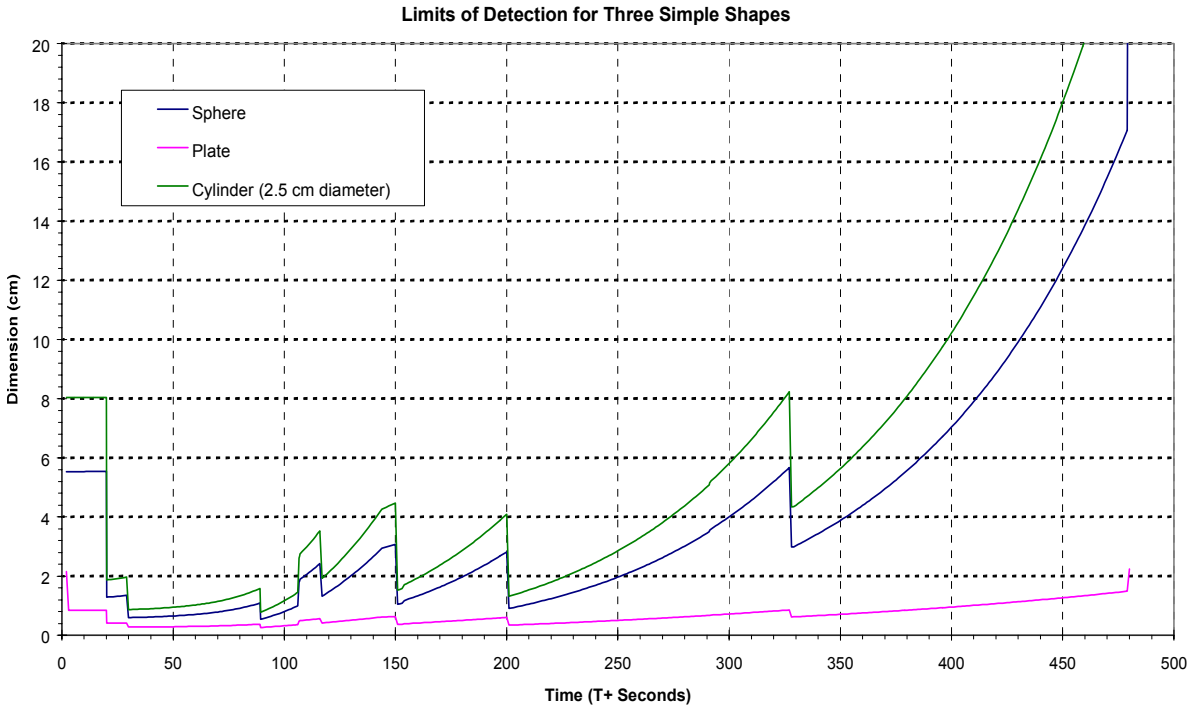

Figure 3-19. Limits of dimensional detectability for three simple shapes

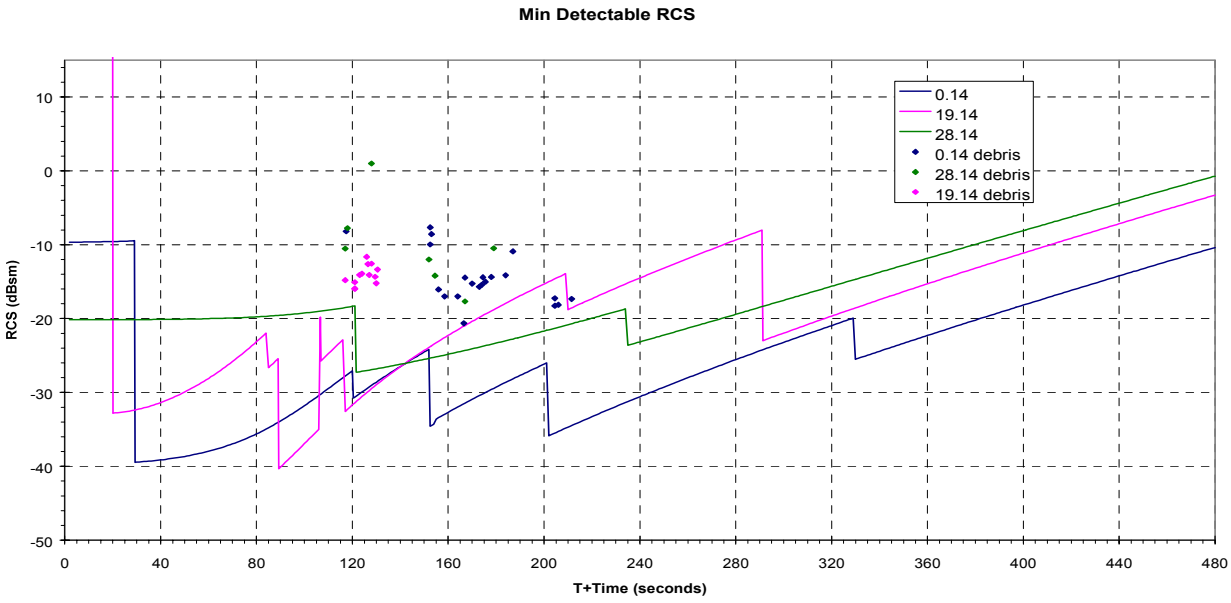

Figure 3-20. Limits of radar cross section (RCS) detectability and measured STS-107 debris for three radar source sites

From Table 3-3, debris item numbers 1 and 29 appear from 80.4 - 87 seconds and 81.6 - 86.1 seconds, respectively. This time coincides with the ET left bipod foam debris generation at 81.7 seconds. However, the low separation rate and relatively large RCS of the two radar objects indicate that they are most likely traveling with the vehicle and are flame (plume) artifacts. There are also several radar objects around the SRB separation time frame, ~126 seconds; however, the data are inadequate to determine the size, shape, or composition of the objects beyond that their moderate separation speed indicates solid objects being left behind. Some known debris objects at the time of SRB separation are the aft Booster Separation Motor (BSM) throat covers. It should be noted that the number and strength of the radar returns are typical as compared to previous Shuttle missions where no significant debris damage occurred.

In an effort to identify the STS-107 launch debris, data was reviewed from a post-STS-27 radar calibration that was performed on several materials. These objects included many applicable Space Shuttle system materials, including various Orbiter thermal protection system tiles, various ET insulation foam types, as well as numerous SRB/SRM materials and potential debris sources. Table 3-4 lists the material samples tested for Orbiter, ET, and SRB/SRM elements. Additionally, data was used from the 2003 Wright Patterson Air Force Base testing, including Orbiter Felt Reusable Surface Insulation (FRSI), High-Temperature Reusable Surface Insulation (HRSI), and HRSI with Room-Temperature Vulcanized (RTV) sealant and Strain Isolation Pad (SIP).

Table 3-4. Material samples from post-STS-27 radar calibration tests

Orbiter	**SRB/SRM**
Black tile	MSA-1/TPS with Hypalon
White tile	MSA-2/TPS with Hypalon
	Cork with Hypalon
ET	Aft booster separation motor (BSM) cover
PDL (closeout foam)	SRM slag
Ice plate	Cork
CPR 488 (acreage foam)	K5NA
Super Light Ablator (SLA) 561M	Instafoam
MA25	Inhibitor
BX250	EA934 adhesive
Instafoam	Viton thermal curtain
	Quartz cloth blanket

As a result of the testing, the minimum detectable size for each radar return for selected materials was determined and catalogued. These data were carefully screened and scrutinized, using some reasonableness tests and assumptions, in an attempt to identify STS-107 radar objects as Orbiter, ET, or SRB/SRM debris.

The radar data are inconclusive with respect to determining identity, size, or shape of any of the debris objects detected. The signal returns were weak and too close to radar noise to allow estimation of object shape. The number and strength of the returns on STS-107 are typical of previous Space Shuttle launches, including those where no debris damage occurred.

3.5 LAUNCH GUIDANCE NAVIGATION AND CONTROL

Postflight analysis of the STS-107 ascent data revealed several events that were within the design capability of the Shuttle, but considered to be new flight experience. These events were reviewed in detail, primarily because they occurred prior to SRB separation, when the foam loss and wing impact were observed. The items considered new flight experience were environmental (wind relative) side-slip angle during the period of maximum dynamic pressure (Hi-Q), SSME yaw nozzle positions during Hi-Q, and SRB thrust mismatch during SRB tail-off. Other events observed during the flight that were not new flight experience, but were considered worthy of note included the presence of a negative orbiter body yaw rate at ET separation and a period of ET slosh during powered ascent. Each event was separated into the following categories for detailed study and evaluation: wind shear, predicted versus actual vehicle loads, ET slosh, nozzle positions, and ET separation yaw rate.

Those parameters along with several other STS-107 ascent Guidance, Navigation, and Control (GNC) related points of interest were studied to determine if they were significant relative to the scenario. The study included integrated vehicle loads analysis, comparison of the STS-107 data with historical flight experience envelopes, and comparison of STS-107 data with specific families of flights. This section of the report summarizes the integrated GNC flight data review.

3.5.1 Wind Shear, Day of Launch Wind Effects

STS-107 experienced a wind shear during the period of maximum dynamic pressure starting at 57 seconds MET (Mach 1.27). The wind shear was due to a rapid change in the out-of-plane wind velocity of -37.7 feet per second over a 1200 foot altitude range starting at approximately 32,000 ft (as shown in Figure 3-21). Immediately after the vehicle flew through this altitude range, its side-slip angle began to increase in the negative direction, reaching a value of approximately –1.75 degrees at 60 seconds. This value of side-slip angle is a new flight experience value for MET 60 seconds (as shown in Figure 3-22). Post-flight data review indicates that the new flight experience side slip event not the result of the wind shear itself. Instead, it was the direct result of a difference in the L - 4:35 minutes balloon measurement, upon which orbiter guidance commands were updated on launch day, and the actual winds flown through by the orbiter during launch and ascent. Figure 3-21 highlights the difference in these two winds in this altitude region (a 25 foot per second increase in out-of-plane magnitude pre-launch compared to a 12 foot per second reduction in magnitude as experienced by the vehicle)

The L - 4:35 minutes weather balloon is launched to measure atmospheric conditions at the launch site, which are then used as part of a standard process to update the orbiter guidance software to keep it within design limits and minimize loads during ascent. After the Day of Launch I-Load Update (DOLILU) software update but prior to launch, additional balloons are used to verify that the L - 4:35 minutes balloon atmospheric conditions are still valid and meet required tolerance checks required to commit for launch. All STS-107 balloon measurements taken on launch day after L - 4:35 minutes

satisfied the required launch commit criteria, and were subsequently verified by balloon data taken 15 minutes after launch.

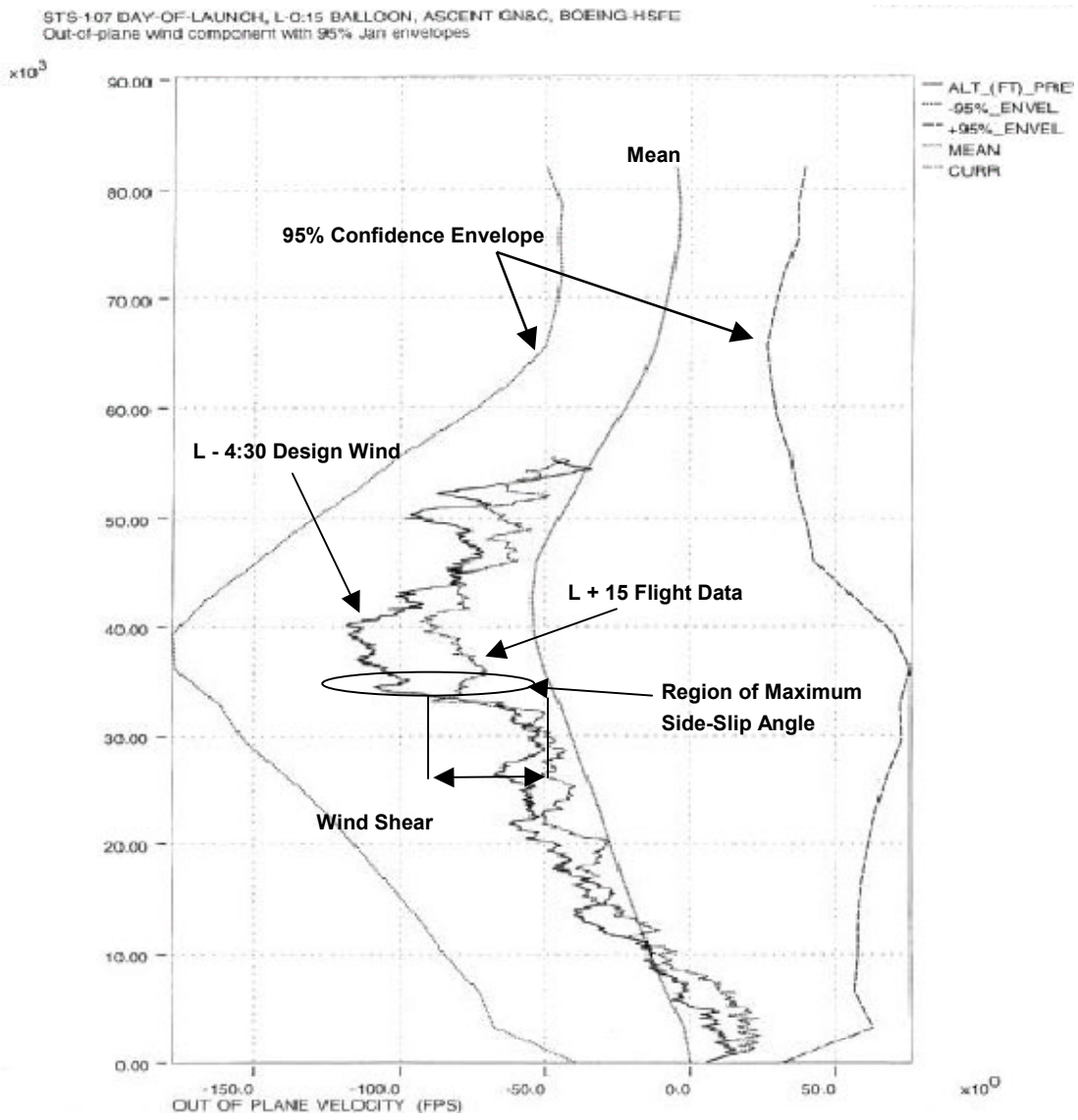

Figure 3-21. Out-of-plane wind velocity

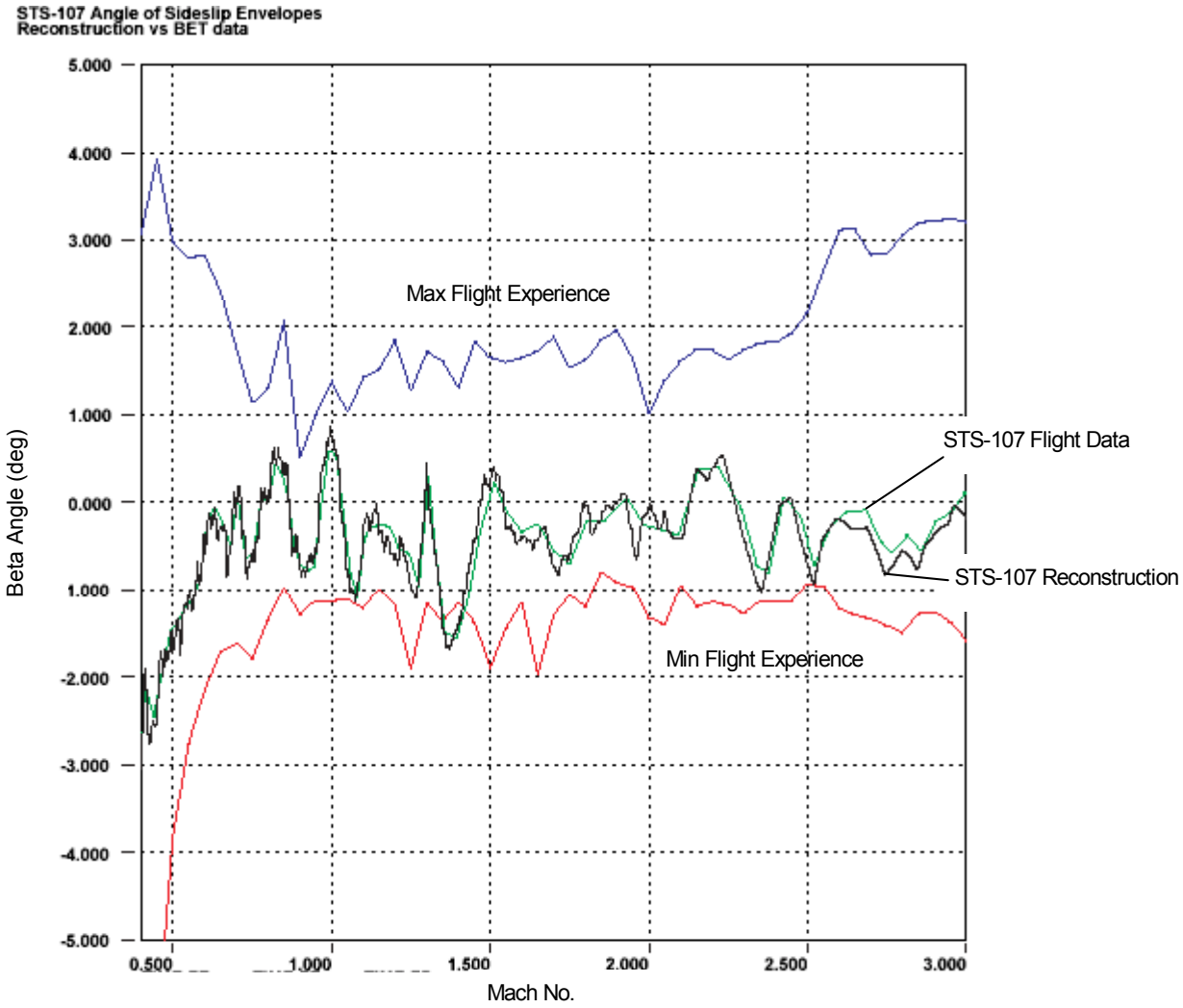

Figure 3-22. Side-slip angle

Several theories consider this wind shear event and the difference between the balloon data to be significant. A negative side-slip angle places the wind vector on the left side of the orbiter, pushing the orbiter to the right, changing the complex aerodynamic flow pattern characteristics in the left ET bipod area. To better understand the conditions on the ET left bipod, several studies were conducted. The studies (1) compared flight data for missions that had ET bipod foam liberation; (2) compared flight data for missions that flew a Light Weight Tank (LWT) in combination with ascent Performance Enhancements (PEs), a package of vehicle software and hardware changes designed to increase overall weight to orbit capability for the ISS; (3) analyzed external aerodynamic loads on the ET forward attach bipod ramp; and (4) studied integrated orbiter/ET vehicle loads.

The flight data correlation studies indicate that a negative side-slip angle during the period of maximum dynamic pressure alone could not explain the liberation of the bipod foam. For both families of flights in the study (LWT and PE flights, and bipod foam liberation flights), a negative side-slip angle was seen on almost every flight. Of the bipod foam loss flights, STS-90 was of particular interest. STS-90 had a larger negative side-slip angle in Hi-Q of -2.0 degrees, when compared to STS-107, yet STS-90 did not lose bipod foam. When flights that shed bipod foam were studied as one family of flights, STS-112 is another outlier that does not support the negative side-slip angle theory. During the STS-112 ascent, video coverage shows the bipod foam liberation occurring prior to Hi-Q, yet the negative side-slip angle on STS-112 did not occur on that flight until after Hi-Q. The details of the flight data correlation studies are summarized in Sections 3.5.6 and 3.5.7 of this report.

To understand the aerodynamic loads on the ET forward attach bipod ramp, a CFD loads assessment was performed. The resulting CFD loads, discussed in more detail in Section 3.5.2, demonstrated that the external aerodynamic loads were below the design requirement.

To measure the orbiter/ET interface loads, an integrated orbiter/ET loads assessment was performed. The assessment, summarized in Section 3.5.2 of this report, also showed all integrated vehicle loads were below design limits.

The day-of-launch wind effects (including the noted wind shear event and associated negative side-slip angle) alone did not cause the ET left bipod foam loss.

3.5.2 Predicted/Actual Loads

Postflight reconstruction analysis of the STS-107 ascent loads characterized the effects of (1) RSRM thrust mismatch, (2) ET slosh dynamics, and (3) wind shear in Hi-Q. The integrated effects of these events were calculated through a flexible body loads assessment. This loads assessment used the STS-107 reconstructed ascent trajectory, and included ET slosh dynamic forces. The assessment produced (1) a wing loads summary, (2) an ET/orbiter interface loads summary, and (3) a summary of external aerodynamic loads on the ET forward attach bipod ramp.

The wing loads analysis used a flexible body structural loads assessment that was validated by the MADS data. The wing loads analysis used reconstructed trajectory parameters to generate the loads on the orbiter wings during ascent. The assessment demonstrated that all orbiter wing loads were 50 to 60% of their design limit, or less, throughout the ascent. This includes the wind shear event at 57 seconds MET, and subsequent side-slip angle at 60 seconds MET (as shown in Figure 3-23).

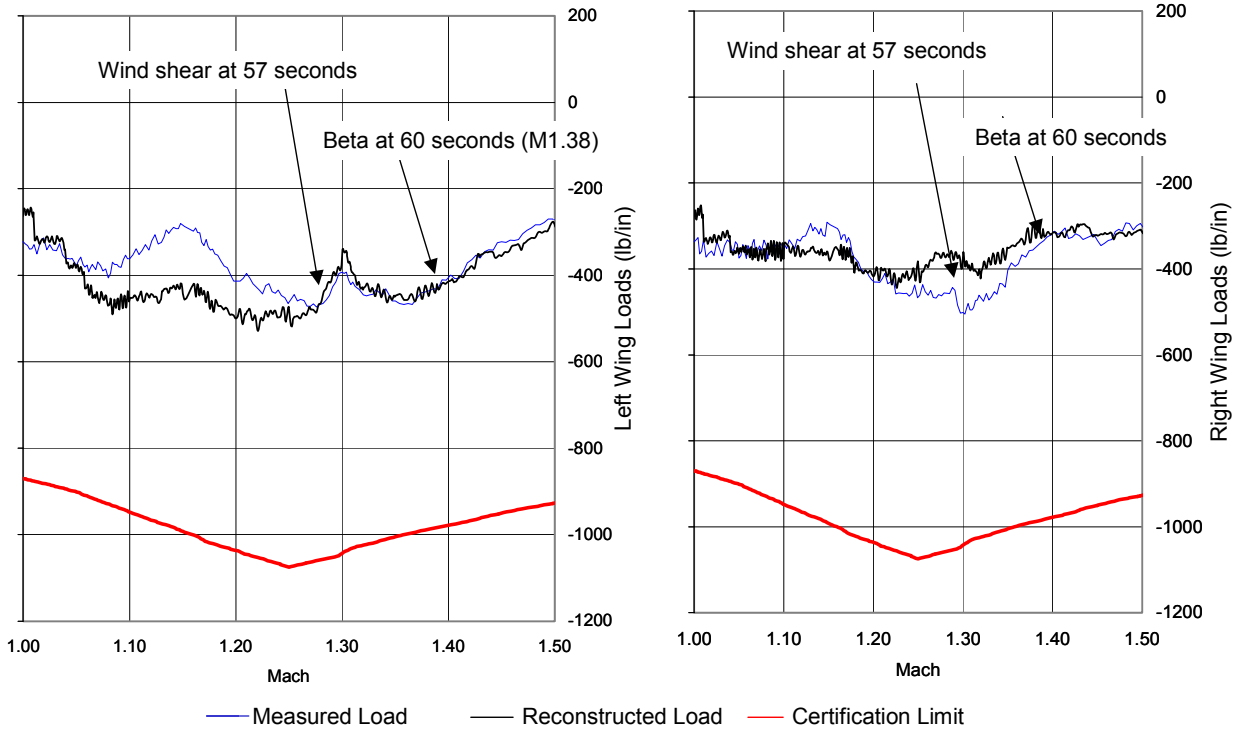

Figure 3-23. Wing loads during wind shear and side-slip angle

The ET/orbiter interface loads were generated using reconstructed trajectory parameters that included the effects of wind shear/crosswind, side-slip angle, and ET liquid oxygen (LOX) slosh. The loads analysis demonstrated that the ET forward attach loads were within certification requirements at all times. The wind shear event had only a small effect on the overall ET loads relative to the required limits (as shown in Figure 3-24), as did the ET liquid propellant slosh (as shown in Figure 3-25). The resulting load from the wind shear event was of the same order magnitude as the roll maneuver and other first stage events prior to SRB separation.

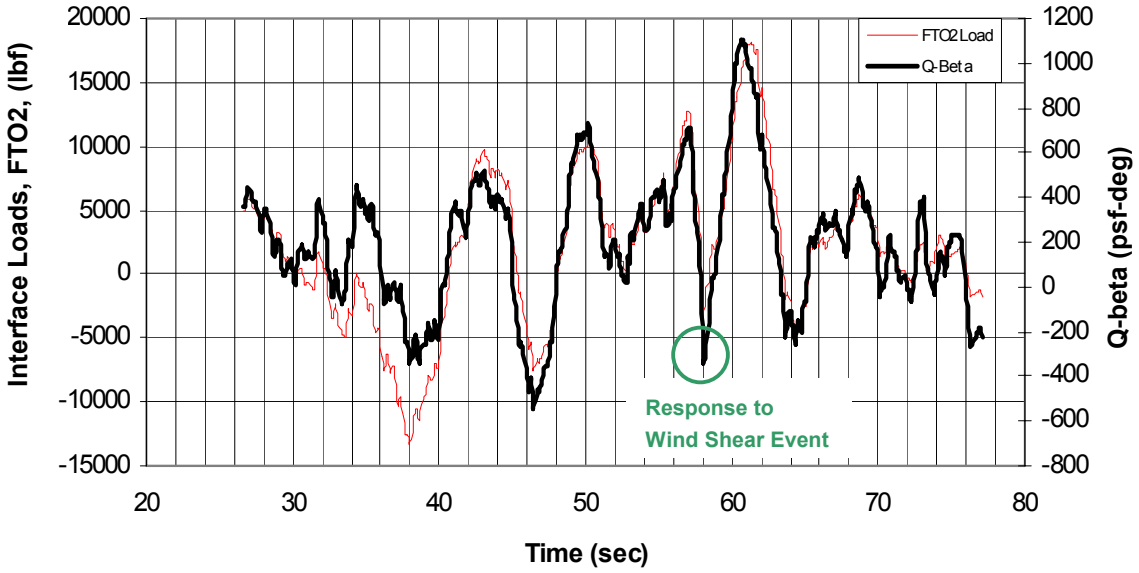

Figure 3-24. ET interface loads at forward attachment during wind shear and side-slip angle. Q-beta is side-slip angle multiplied by the dynamic pressure and represents the side-slip angle contribution of the interface load

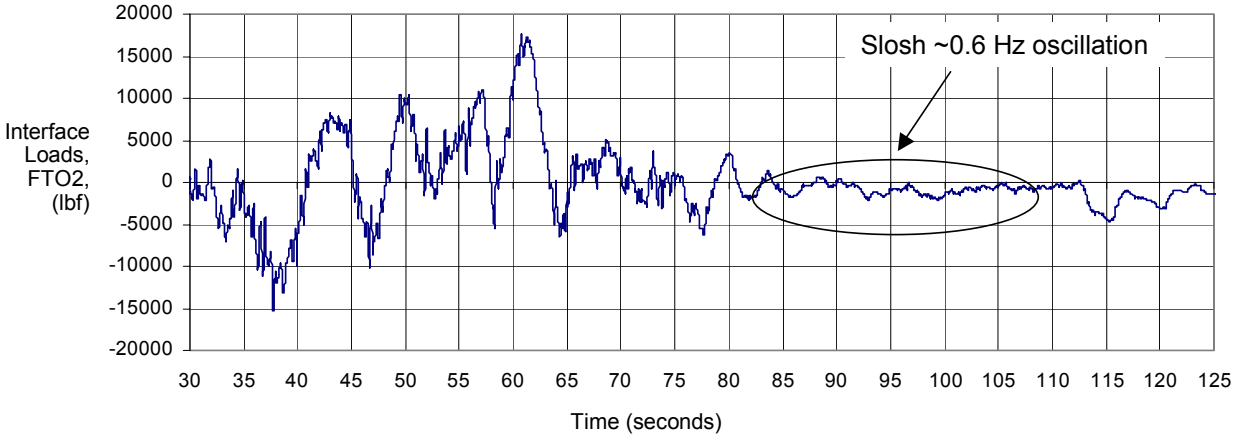

Figure 3-25. Slosh effect on ET interface loads

The external aerodynamic loads on the ET forward attach bipod were analyzed using a CFD simulation. The simulation produced axial, side-force, and radial loads as shown in Figure 3-26, Figure 3-27, and Figure 3-28, respectively. The CFD assessment of the bipod area indicated that the external air loads were below the design limit during the Hi-Q region and at the time of the bipod foam liberation.

Flexible body simulation results indicate that all vehicle elements and associated loads were within required limits. The reconstruction loads analyses indicate that the ascent environment-induced loads alone did not cause the ET bi-pod foam loss.

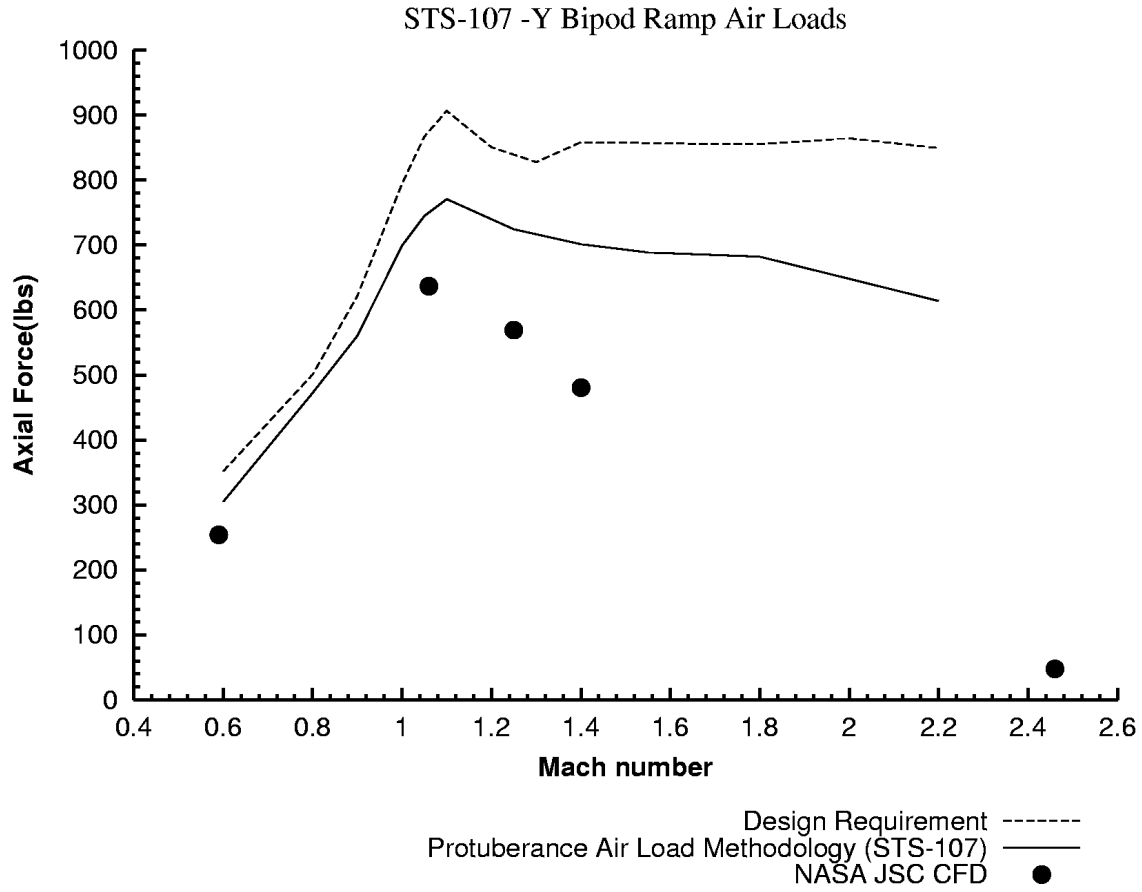

Figure 3-26. ET bipod axial aerodynamic loads

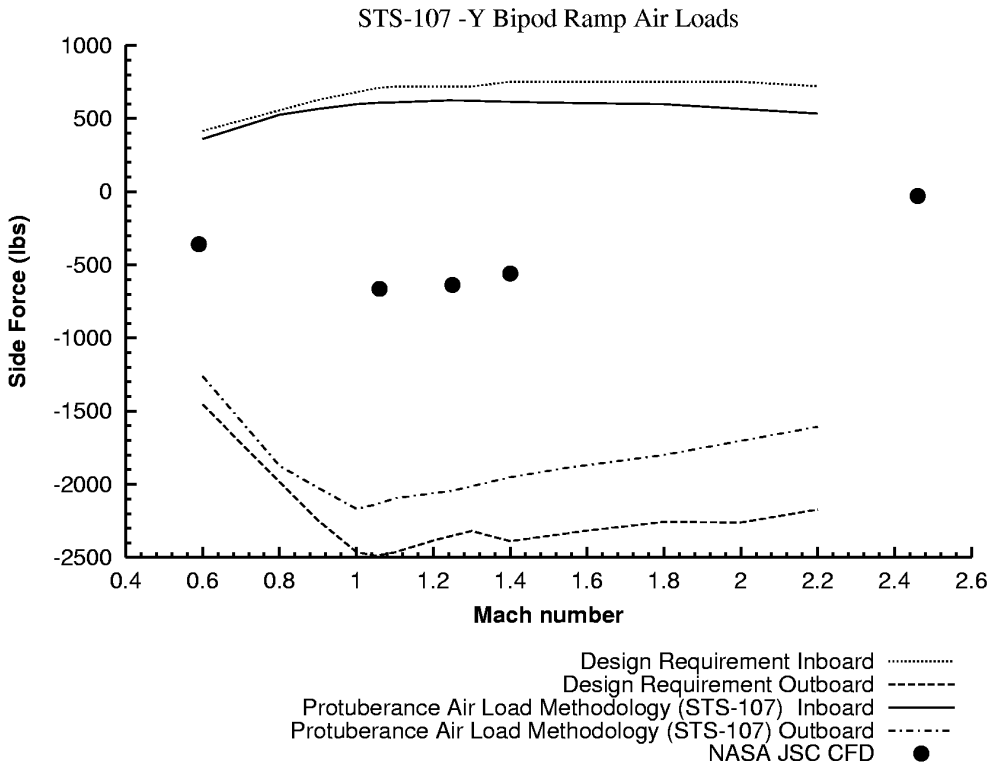

Figure 3-27. ET bipod side-force aerodynamic loads

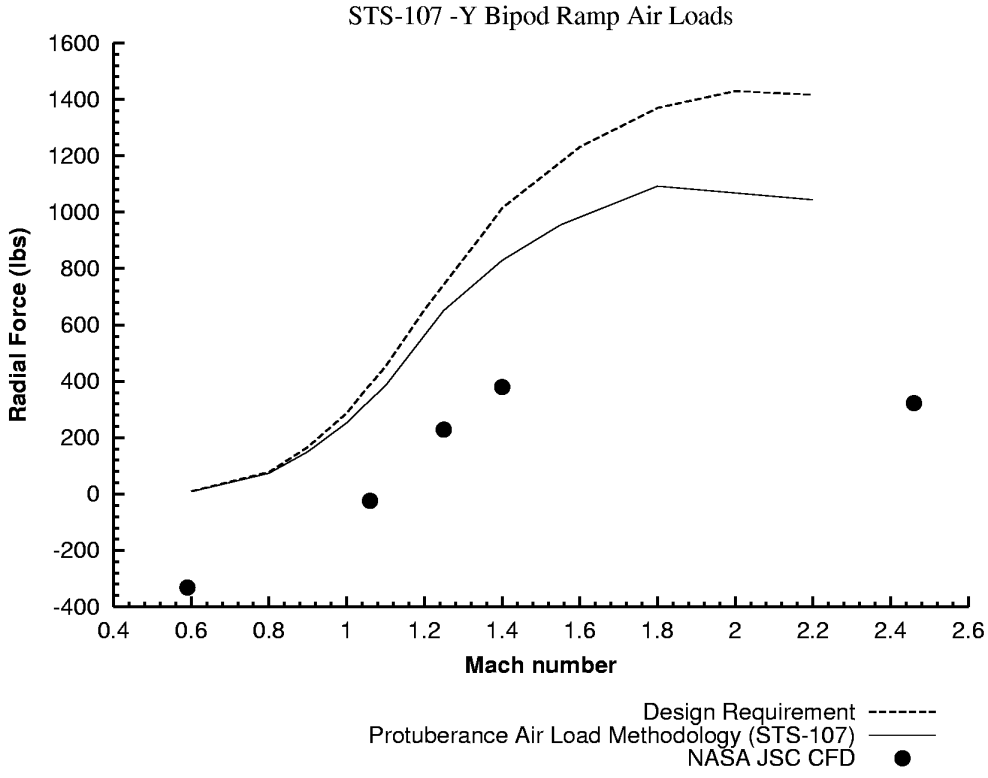

Figure 3-28. ET bipod radial aerodynamic loads

3.5.3 ET Liquid Oxygen Slosh

The STS-107 ascent data indicate a 0.6 Hz actuator oscillation frequency that peaks in amplitude at 55 seconds, and again at 77 seconds MET and continues through SRB separation. The peaks directly correlate to peaks in 0.6 Hz wind content. A 0.6 Hz oscillation in the Flight Control System output is of interest since it can couple with the ET Liquid Oxygen (LOX) slosh mode. Slosh refers to the repeated side-to-side movement of the center of gravity of the liquid oxidizer propellant in the external tank. The slosh mode frequency and amplitude cannot be measured directly through vehicle data. In order to determine if ET LOX slosh is present, a post-flight process of reviewing the vehicle SRB and SSME actuator frequency content must be conducted, as well as that of the launch wind. When this post-flight process was conducted for STS-107, it revealed that this flight experienced more than typical 0.6 Hz frequency content in the SRB tilt actuators with moderate content in the rock actuators. Figure 3-29 illustrates this point with the results of the SRB left tilt actuator frequency response as compared to previous Columbia flight history.

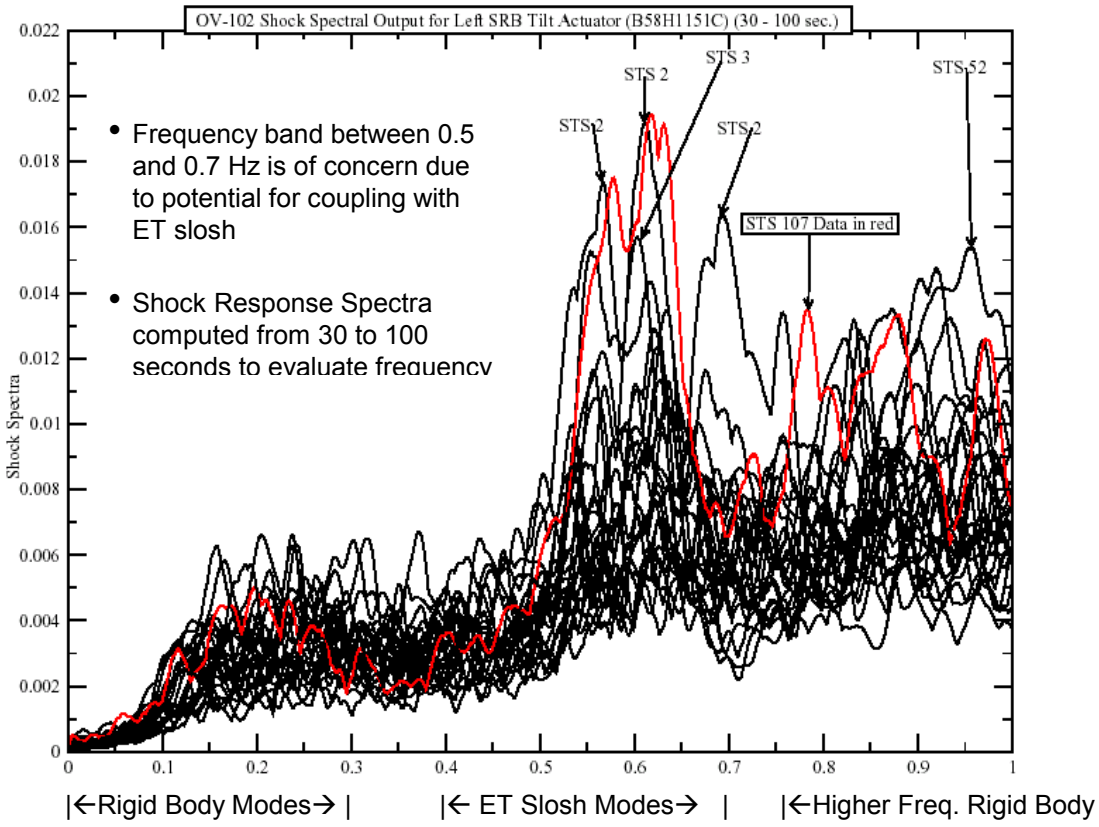

Figure 3-29. STS-107 SRB tilt actuators experienced more than typical 0.6 Hz content

Figure 3-30 shows the relative time variation of amplitudes of the 0.6 Hz frequency content in wind and actuator data. The close correlation between the peaks in the 0.6 Hz content of the right and left actuator responses and the wind dynamics indicates that the actuators were responding primarily to wind rather than ET LOX slosh at this frequency through most of first stage (prior to SRB separation). As the 0.6 Hz content of the wind dynamics reduces in magnitude late in first stage, the remaining 0.6 Hz content in the actuator response may be attributed to a combination of the remaining wind dynamics and low-amplitude ET LOX slosh. STS-90 shows a similar wind frequency content.

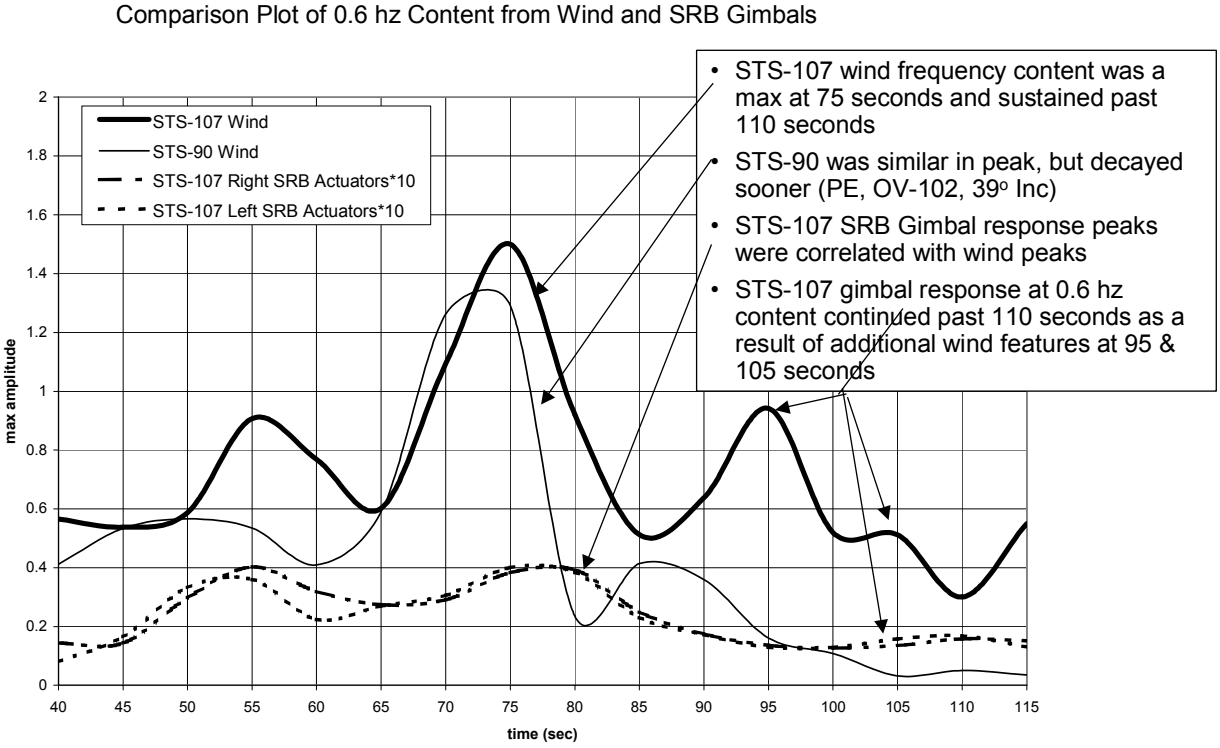

Figure 3-30. STS-107 SRB gimbal responses at 0.6 Hz frequency correlated to wind

In general, ET LOX slosh is due to (1) commanded vehicle attitude transients, (2) additional wind dynamics after the start of ET LOX slosh, and (3) the 0.2 Hz rigid body vehicle mode. Note that a 0.6 Hz mode is the 3rd harmonic of the 0.2 Hz frequency, and is therefore subject to cross-coupling, and that some wind conditions can naturally contain a 0.6 Hz content.

The data from the ET LOX slosh study indicate that the flight control system operated as designed, and that more than adequate slosh phase stability margin existed. When the ET LOX slosh data is combined with the integrated vehicle loads analysis results (reference Figure 3-25), data indicate that the ET LOX slosh did not result in excessive vehicle loads at the orbiter/ET interface.

3.5.4 Nozzle Positions

A review of the STS-107 ascent data identified two discrete points in time when the SRB and SSME nozzle positions exceeded the flight experience envelope for those respective times in the ascent profile. The first event occurred when the center and right SSME yaw deflections exceeded the previous flight experience envelope during the period of maximum dynamic pressure, as a result of the differences between predicted and actual flight wind conditions (as shown in Figure 3-31 and Figure 3-32).

This nozzle yaw event was coincident with a wind-inducted positive lateral acceleration, as sensed via the body mounted accelerometer assemblies and a positive orbiter body yaw rate, as sensed by the orbiter rate gyro assemblies. The yaw event follows the period of greatest change in out-of-plane wind velocity (e.g., the wind shear previously shown in Figure 3-21).

The large offset in the Center and Right SSME yaw positions at 62 seconds MET was the reaction of the flight control system to the wind shear event and day-of-launch wind differences as compared to the DOLILU design. The nozzle motion was within the capability of the Shuttle flight control system, and the system operated as designed. As discussed in Section 3.5.1, the reconstruction loads analyses indicate that the ascent environment-induced loads alone did not cause the ET bipod foam loss.

The second nozzle motion event occurred when the SRB and SSME Thrust Vector Control (TVC) pitch and yaw deflections exceeded the previous flight experience envelope during SRB tail-off (as the SRB thrust diminished). The new flight experience envelope for the SSME and SRB nozzle positions was primarily due to (1) low Reusable Solid Rocket Motor (RSRM) performance that caused a time shift of the SRB tailoff events relative to previous flight experience, as indicated by a low burn rate shown in Figure 3-33, (2) a thrust mismatch between the left and right SRB caused by lower than normal thrust on the right SRB during tail-off, the final seconds of SRB burn (as shown in Figure 3-34), (3) a small bias in the left SRB pitch actuator that shifted the actuator positions farther toward the edge of the flight experience envelope, and (4) flight control trim characteristics unique to PE flights (as shown in Figure 3-35).

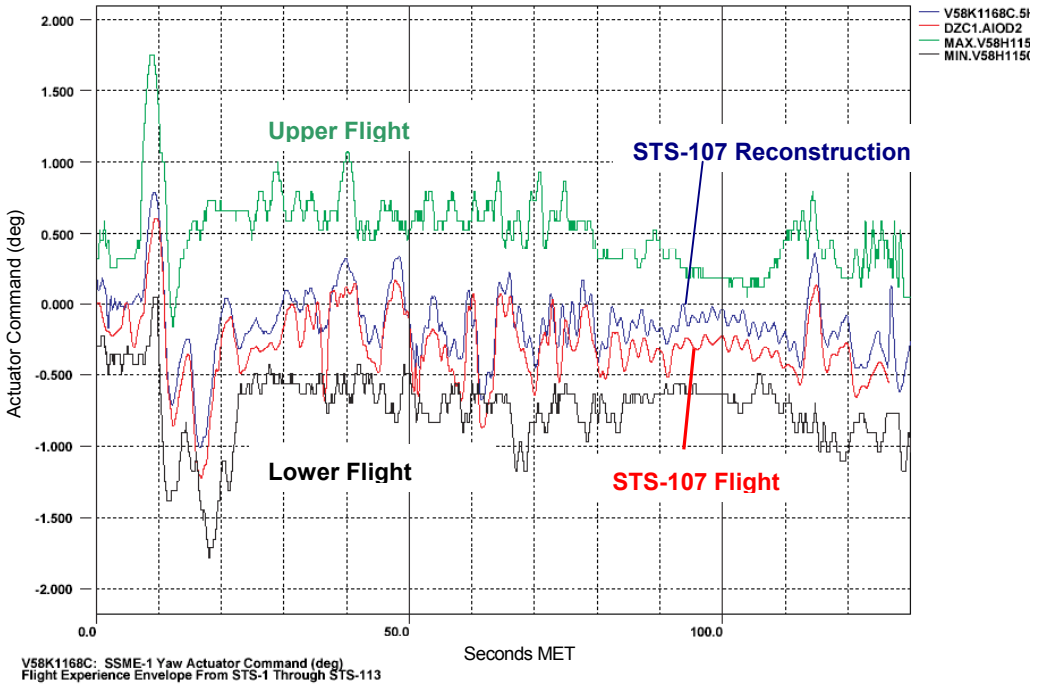

Figure 3-31. Center SSME yaw position

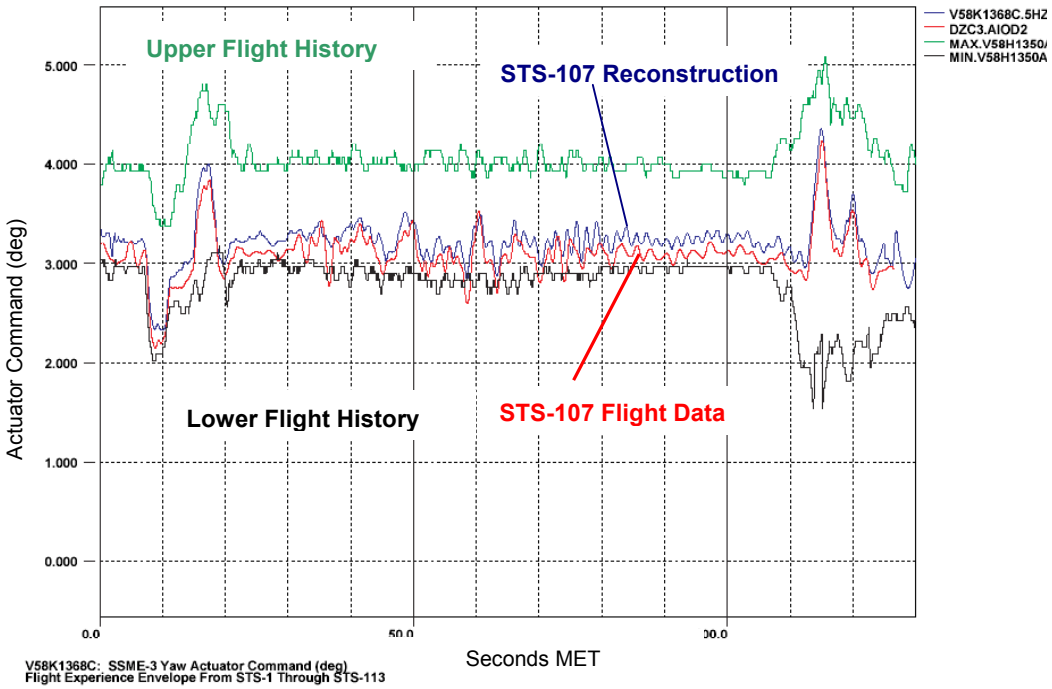

Figure 3-32. Right SSME yaw position

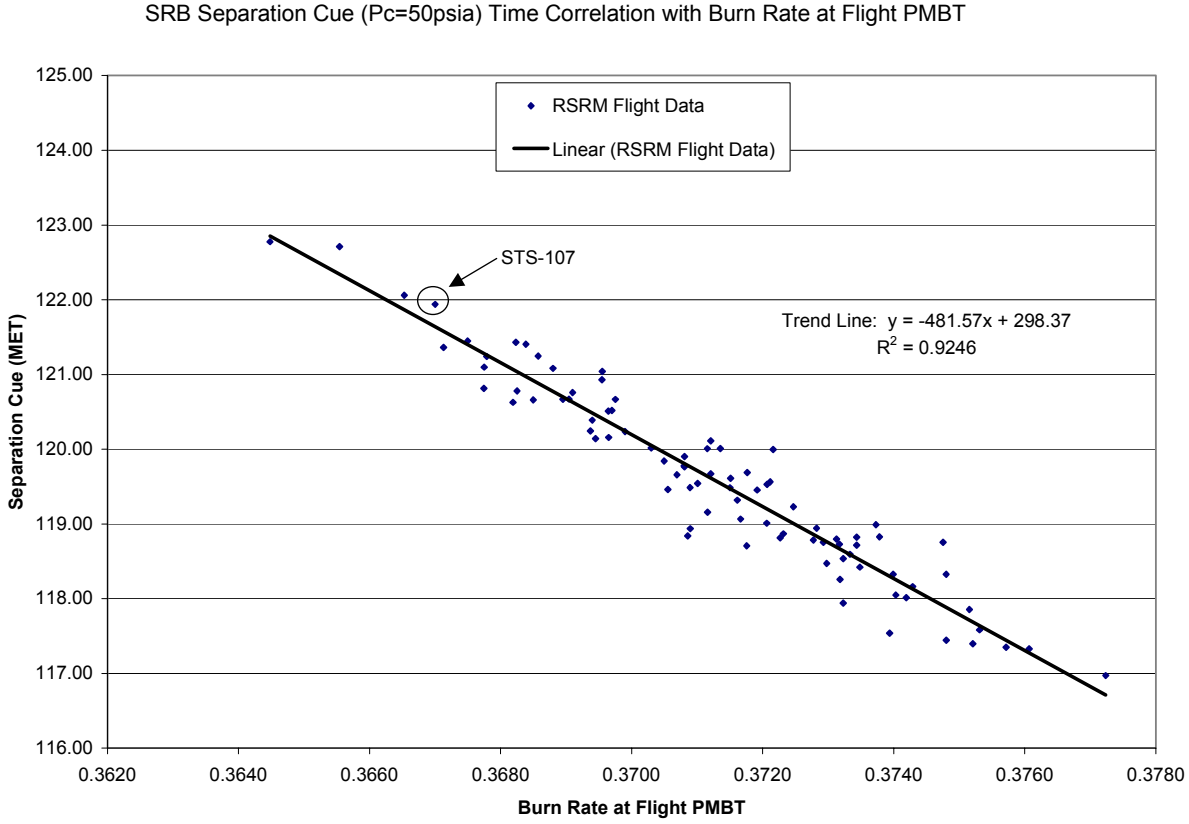

Figure 3-33. RSRM burn rate at propellant mean bulk temperature (PMBT)

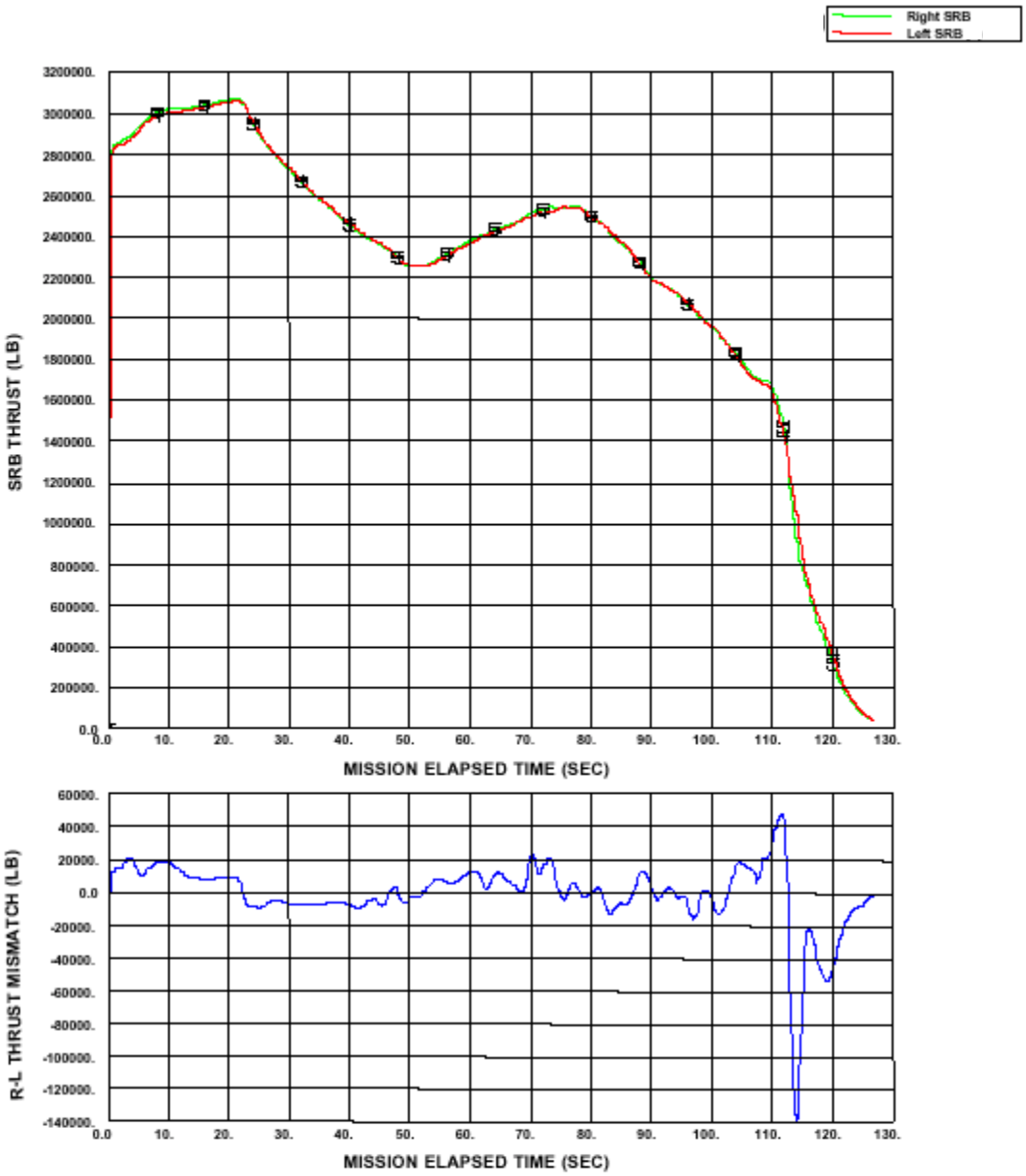

Figure 3-34. SRB thrust mismatch

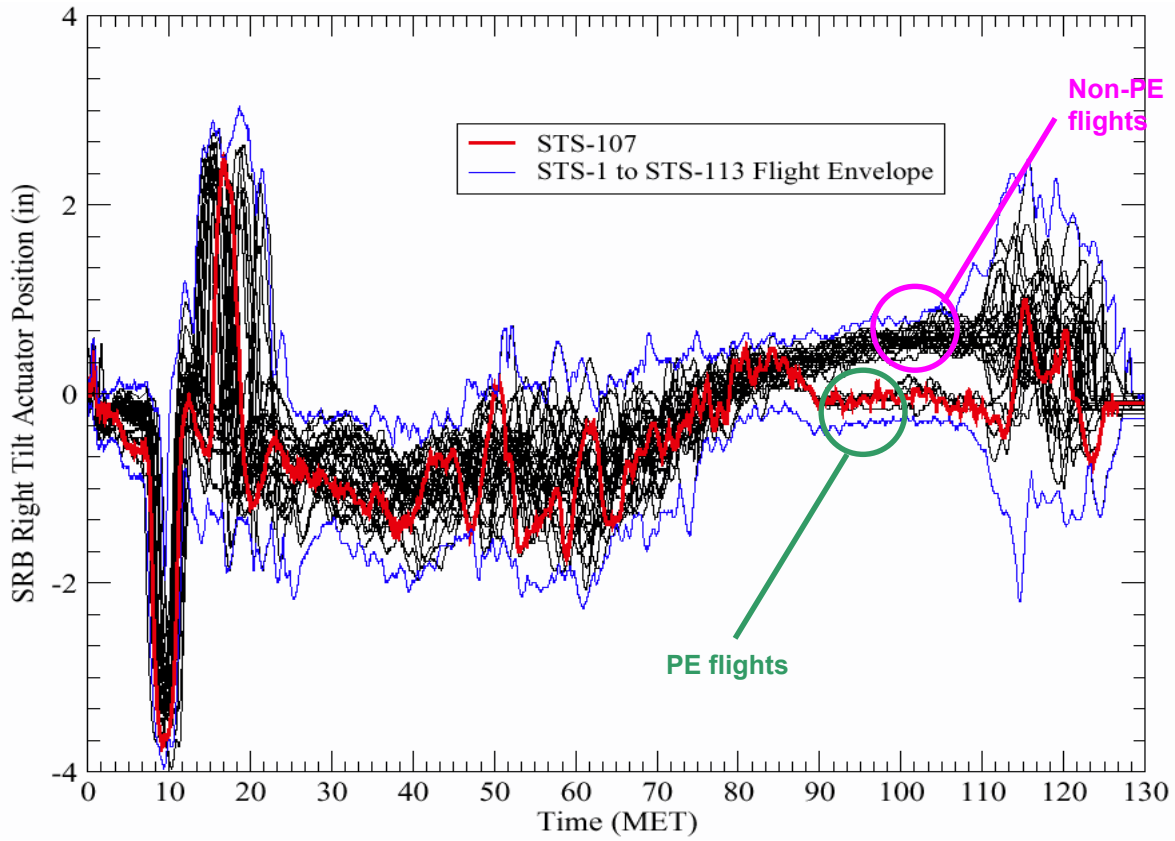

Figure 3-35. SRB nozzle position for PE flights versus non-PE flights

The RSRM burn rate is a temperature dependent function, and are determined based on pre-flight tests of small samples of the actual motor propellant at a reference temperature. These values are then adjusted based on a Predicted Mean Bulk Temperature (PMBT) based on the actual weather conditions prior to launch day. For STS-107, the pre-flight predicted motor performance was very close to that determined by post flight reconstruction. A low RSRM burn rate does not affect the total impulse produced by the RSRM during first stage; it only affects the amount of time the RSRMs must burn to achieve the same level of impulse.

The SRB thrust mismatch observed during tail-off was well within the design margin of the flight control system, and similar occurrences have happened numerous times during previous flights.

Due to flight control gain settings unique to PE flights, PE flights have a nozzle position closer to zero inches deflection from 85 to 110 seconds MET. The flight data that coincides with the STS-107 data are all from PE flights, seen clearly in the 85 to 110 seconds MET timeframe in Figure 3-33. The other grouping of flights in this same timeframe (85 to 110 seconds MET) are all non-PE flights and have larger pitch nozzle deflections.

To examine if SRB thrust mismatch during tail-off contributed to the loss of the ET bipod foam, several studies were conducted. The studies included data correlation of

(1) flights that used LWT and PEs, and (2) flights that shed ET left bipod foam. The data correlation showed that for both families of flights, SRB thrust mismatches were observed on the majority of flights. The only flights to not have significant SRB thrust mismatches near SRB tail-off were STS-87 and STS-90. The study of the two families of flights are summarized in Sections 3.5.6 and 3.5.7 of this report.

The data indicate that the SRB thrust mismatch on STS-107 was a direct result of SRB burn rate differences between the left and right SRB. The thrust mismatch observed on STS-107 and the new flight experience nozzle positioning occurred after the foam shedding event. The SRB thrust mismatch occurred on the majority of flights in both families of flights, including those that did not shed foam.

3.5.5 ET Separation Yaw Rate

A higher than typical negative yaw rate was observed at ET separation during STS-107. The yaw rate, shown in Figure 3-36, was approximately -0.12 deg/sec and near the edge of the flight experience envelope. The negative yaw rate is noteworthy because it does not correspond to the flight control system's thruster activity, known vent forces, or any other explained mission activity. Furthermore, the rate appears at the time of physical separation between the orbiter and external tank, which indicates that it is related to the structural release between the two objects. Although the negative yaw rate was unusual, it was well within the design and certification envelope for ET separation. This rate was also well within the flight limits (± 0.7 deg/sec) for ET separation to occur.

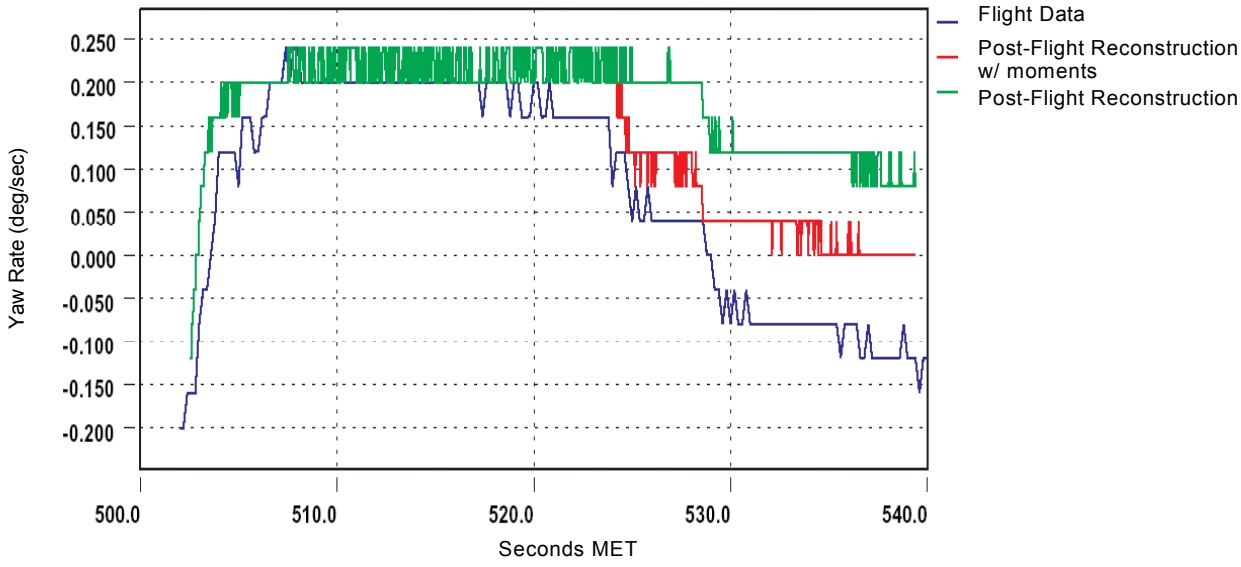

Figure 3-36. ET separation yaw rate

A fault tree analysis narrowed down the cause of the negative yaw rate to a release of strain energy at ET separation due to either (1) a misalignment of the orbiter and external tank at structural mating, or (2) a build up of strain energy in the ET structure

and associated orbiter attachment strut areas due to thermal differences. STS-107 was one of six flights to have a negative yaw rate at ET separation. The other flights with negative yaw rates at ET separation were STS-2, STS-70, STS-80, STS-92, and STS-98. None of these flights are known to have had bipod foam loss. The ET sep yaw rate on STS-2 was identical to that on STS-107, within the 0.02 deg/sec accuracy limits of the sensors and related data and signal noise.

Data indicate that the yaw rate at ET separation did not result in re-contact between the orbiter and the ET after separation. This observation is based on high rate telemetry (25 Hertz) orbiter body rate data, and MADS accelerometer data analyzed post-flight. The yaw rate was within the expected range of vehicle body rates when taking into account all known error sources, including rate sensor noise. The data indicates that no correlation exists between observed yaw rate at ET separation and bipod ramp foam loss.

3.5.6 Data Correlation of Flights that Used a LWT and PEs

To determine if any of the items considered new flight experience were unique to the use of Light Weight (LWT) ET and Performance Enhancements (PEs), an evaluation was performed to compare the STS-107 flight data to other flights using LWT and PEs. The STS-107 data was compared to flights STS-87, STS-89, STS-90, and STS-99 (as shown in Table 3-5).

Table 3-5. LWT and PE flights

Flight	Tank type	ET #	Orbiter	Flight software	Inclination	Launch date
STS-87	LWT	89	Columbia	OI-26A	28.45 deg	11/19/97
STS-89	LWT	90	Endeavour	OI-26A	51.6 deg	1/22/98
STS-90	LWT	91	Columbia	OI-26B	39.0 deg	4/17/98
STS-99	LWT	92	Endeavor	OI-27	57.0 deg	2/11/00
STS-107	LWT	93	Columbia	OI-29	39.0 deg	1/16/03

LWT and PEs were also used on STS-85 and STS-86. Neither flight was included in the LWT and PE flight data correlation study because the flights were the first to use the new PE flight software, and as such had very few of the PEs active. One of the most significant PE's not active for STS-85 and STS-86 was the first stage pitch parallel change. Not having the first stage pitch parallel PE in place resulted in STS-85 and STS-86 being outliers when compared to the other five flights, due to significantly different SRB and SSME nozzle positioning during first stage (as previously shown in Figure 3-35).

The LWT and PE flight data correlation study compared the STS-87, STS-89, STS-90, STS-99, and STS-107 flight data for parameters that were considered new flight experience for STS-107. The LWT and PE flight data correlation included a

comparison of environmental side-slip angle during Hi-Q, SSME yaw position during Hi-Q, SRB thrust mismatch during Hi-Q, ET separation yaw rate during Hi-Q, and ET slosh.

The LWT and PE flight correlation study indicated that negative side-slip angles of -0.75 degrees or more occurred on all flights, including STS-90, which had the second largest side-slip angle of any flight in Hi-Q of -2.0 degrees. Evaluation of SSME yaw positions during Hi-Q indicated that only STS-90 had a similar signature. The STS-90 SSME yaw was primarily due to a large wind shear on that flight. Evaluation of SRB thrust mismatch shows a similar thrust mismatch and corresponding SRB and SSME TVC gimbal activity on STS-89 and STS-99 only. Within this family of flights, the negative yaw rate at ET separation and ET slosh characteristics were only observed on STS-107.

Of all of the flights studied, STS-90 and STS-107 were the most similar. Both flights were flown on Columbia, on a 39.0-degree inclination trajectory, used LWT and PE's, were daytime launches, and had a SPACEHAB module as the primary payload. Furthermore, STS-90 and STS-107 flew through a large wind shear during the Hi-Q region.

The data is inconclusive as to whether ascent GNC parameters/events correlated for flights using a combination of LWT and PE's.

3.5.7 Data Correlation of Flights with ET Bipod Foam Liberation

To examine if any of the items considered new flight experience for STS-107 contributed to the ET bipod foam liberation, a flight data correlation study was performed for all flights known to have lost ET bipod foam during ascent. The flights compared to STS-107 below included STS-7, STS-32, STS-50, STS-52, STS-62, and STS-112 (as summarized in Table 3-6). These are the only flights to have definitive photographic information to show ET bipod foam loss between liftoff and ET separation. An estimate of the ET bipod foam volume obtained from this photographic evaluation can also be found in Table 3-6. It should be noted that STS-32 is under review as a flight that lost ET bipod foam. It is known that STS-32 lost ET foam, but it is not clear at this time if it was acreage foam or bipod foam.

The ET bipod foam liberation flights were compared for parameters that were considered new flight experience for STS-107. The data correlation study included a comparison of environmental side-slip angle during Hi-Q, SSME yaw position during Hi-Q, SRB thrust mismatch during thrust tail-off, ET separation yaw rate, and ET slosh.

The negative side-slip angle of -1.5 degrees or more occurred on all flights in this family, and STS-62 had the largest side-slip angle of any flight in first stage (prior to SRB separation) at -2.5 degrees. Evaluation of SSME yaw positions in first stage show similar signatures occurred on STS-50, STS-52, and STS-62 (all primarily due to large wind shears). Evaluation shows that similar thrust mismatch and corresponding SRB and SSME TVC gimbal activity occurred on all flights in this family. STS-107 is the only

flight in this family to have a negative yaw rate at ET separation. The ET slosh characteristic was present on STS-32, STS-50, STS-52, STS-62, and STS-107.

In summary, the negative side-slip angle and SRB thrust mismatch were evident for all flights on which ET bipod foam loss was observed. For other parameters within this family of flights, no correlations are evident. It is noteworthy that five of the seven flights in the foam loss family were Columbia missions, all with the ET slosh characteristic. Finally, the data are inconclusive as to whether any of the new flight experience parameters (individually, or in some combination) by themselves caused bipod foam loss.

Table 3-6. STS flights with ET left bipod foam liberation

FLIGHT	STS-7	STS-32	STS-50	STS-52	STS-62	STS-112	STS-107
BIPOD FOAM LIBERATED ON ASCENT	***YES***	***Under Review***	***YES***	***YES***	***YES***	***YES***	***YES***
APPROX. DEBRIS VOLUME (cu. in.)	***404***	***295***	***707***	***15***	***1***	***202***	***1200***
ET #	06	25	45	55	62	115	93
ET TYPE	SWT	LWT	LWT	LWT	LWT	SLWT	LWT
ORBITER	Challenger	Columbia	Columbia	Columbia	Columbia	Atlantis	Columbia
INCLINATION	28.45 deg	28.45 deg	28.45 deg	28.45 deg	39.0 deg	51.6 deg	39.0 deg
LAUNCH DATE	06/18/83	01/09/90	06/25/92	10/22/92	03/04/94	10/07/02	01/16/03
LAUNCH TIME (LOCAL)	07:33:00 AM EDT	07:35:00 AM EST	12:12:23 PM EDT	1:09:39 PM EDT	08:53:00 AM EST	3:46:00 PM EDT	10:39:00 AM EDT
SIDE-SLIP ANGLE DURING FIRST STAGE	***YES***	***YES***	***YES***	***YES***	***YES***	***YES***	***YES***
NOZZLE YAW DURING FIRST STAGE	No	No	***YES***	***YES***	***YES***	No	***YES***
SRB THRUST MISMATCH	***YES***	***YES***	***YES***	***YES***	***YES***	***YES***	***YES***
ET SLOSH	No	***YES***	***YES***	***YES***	***YES***	No	***YES***
NEGATIVE YAW RATE AT ET SEP	No	No	No	No	No	No	***YES***

4.0 ORBIT

4.1 INTRODUCTION

While Columbia was on-orbit, there was no indication of damage from either the ascent foam impact or a micrometeoroid/orbital debris (MMOD) hypervelocity debris impact based on orbiter telemetry, crew downlinked video and still photography, or crew reports. Multiple comprehensive postflight reviews of the same data indicated that there was nothing unusual with any of Columbia's systems or structure. This included a detailed review of orbiter Inertial Measurement Unit (IMU) accelerometer, body rates, and jet firing data to determine if there were indications of an orbital debris hypervelocity impact. The results of this analysis show that there were no indications of an orbital debris impact, although there are several unexplained events. Data from an additional accelerometer package, known as Space Acceleration Measurement System (SAMS), was used to determine if this more sensitive system was able to detect any unusual activity during these timeframes. Details of the orbital debris analysis can be found in Section 4.2 and the flight day 2 debris event will be discussed in Section 4.3.

4.2 ORBITAL DEBRIS

4.2.1 Orbital Debris Risk Assessment

There were multiple payload constraints on this mission, which resulted in 239 attitude maneuvers, or orientation changes. For each Shuttle mission the complement of attitude maneuvers is analyzed for orbital debris risk of a critical penetration due to an on orbit hypervelocity impact. This same analysis, performed post-flight, determined that the probability of no critical penetration was 0.9972, which is well below the guideline for critical penetrations. The analysis also included specifics for critical penetrations of the left wing. The results show that the overall probability for no critical penetration is 0.9996 for the entire left wing and 0.9999 for the left wing leading edge RCC.

4.2.2 Micrometeoroid or Orbital Debris Detection

Postflight, a NASA JSC team consisting of members from Mission Operations, Engineering, and Space and Life Sciences with the support of Draper Labs, participated in an effort to use downlisted data to identify any external forces or torques that could be correlated with an MMOD impact. This task was divided into four different areas:

1. Build an inclusive, detailed activity timeline that includes all known Shuttle and payload events (venting, waste control system activities, LiOH canister change out, payload bay door operations, and SPACEHAB systems operations) that would cause attitude and rate errors or momentum changes detectable by the orbiter systems.

2. Review the orbiter IMU rate data for net changes in angular momentum, which would be indicative of an MMOD strike.

3. Screen the 20,000 plus orbiter Vernier Reaction Control System (VRCS) jet firings with an algorithm to determine whether or not each firing was due to the control system response to normal attitude changes or disturbances, or in response to an MMOD strike.

4. Examine SAMS payload experiment data for potential signs of an MMOD strike.

4.2.2.1 IMU Rate Data Review

This study reviewed all orbiter data from various sensors and systems. The only data useful for this study were the orbiter body axis rate data, which are derived from IMU attitude data by the Guidance Navigation and Control (GNC) flight software. This analysis assumed rigid body dynamics; flexural response was covered in the SAMS data analysis (see below).

The entire orbit portion of the mission, from the orbit transition (1 hour MET) to four hours prior to the deorbit, was examined. A total of 238 events of interest were identified which required further examination. All but 13 of these events were correlated to either a known forcing function, or the signature did not match the expected dynamic response of an externally applied impulse (MMOD strike). The remaining 13 unexplained events were analyzed in significantly greater detail.

Additional analysis included the evaluation of the rate transients and a time integration of the change in angular momentum across the event of interest. The guiding principle of this analysis is that unless there is an external force or torque applied to the vehicle, conservation of angular momentum will always apply. This study resulted in the elimination 10 of the 13 events that did not fit the expected response for an externally applied impulse. One event was inconclusive due to the low resolution of the data, and the remaining two events have the potential to be caused by an MMOD strike; however, other causes are also possible (unknown venting, etc.). The orbiter rate data cannot be used to explicitly determine mass, velocity, or point of impact of an MMOD object. Table 4-1 provides an overview of the original 13 events of interest.

Table 4-1. Summary of analysis of 13 rate events

Event	EST* (Day:hour:min:sec)	MET* (Day:hour:min:sec)	External torque, unknown venting, or potential MMOD** strike	Angular momentum conserved (crew motion, other, or unknown)	H_2O dump	Inconclusive
1	18/11:45:00	2/01:06:00		X		
2	19/12:45:50	3/02:06:50		X		
3	19/20:02:20	3/09:23:20	X			
4	19/21:31:30	3/10:52:30		X		
5	24/16:45:10	8/06:06:10			X	
6	25/04:19:20	8/17:40:20	X (possible)			
7	25/05:08:00	8/18:29:00		X		
8	26/03:53:20	9/17:14:20		X		
9	29/00:02:00	12/13:23:00		X		
10	29/15:48:30	13/05:09:30		X		
11	29/17:40:10	13/07:01:10		X		
12	31/11:07:00	15/00:28:00				X
13	32/02:02:30	15/15:23:30		X		

* Times are approximate

** Micrometeorite or orbital debris

4.2.2.2 Lower Bound of IMU MMOD Detection Threshold

Two separate techniques were evaluated to attempt to bound the lowest MMOD mass and velocity that could be detected using the orbiter IMU data. The first used measured angular rate data, while the second used the accelerometers to measure a change in velocity.

There were two assumptions for this angular rate analysis. First, the lowest value of angular rate change that can be detected by the Shuttle IMU's is 0.002 deg/sec, based on an evaluation of body rates and engineering judgment. Second, to bound the minimum mass of an MMOD object, the efficiency of transfer of linear momentum of the striking object was assumed to be 100% with optimal geometry. The resulting transfer of the linear momentum is a change of orbiter angular momentum.

The bounding of the lower limit of the linear momentum and/or mass of a potential strike object is not a one-dimensional exercise. Several assumptions must be made to perform this analysis. Strike location on the orbiter is significant. For a fixed orbiter rate change from a strike, the radius from the orbiter center of gravity (CG) to the strike location is inversely proportional to the linear momentum of the striking object. Also, once the linear momentum of the striking object is defined, the mass of the object is inversely proportional to the velocity. The examples shown in Table 4-2 are three of many possible solutions; however, they have been selected to be representative of a strike location roughly associated with the main landing gear door and forward through the leading edge of the wing.

Table 4-2. Summary of analysis of the lower bound of MMOD (based on body rate data)

Body Axis	Body Rate (degrees per second)	Angular Momentum (slug*ft^2/sec)	Assumed Strike Location of MMOD	Assumed Velocity of MMOD (nmi/sec)	Lower Bound of the Mass of MMOD *(Assumes optimal geometry & 100% momentum transfer)* (gram)
Roll	0.002	36	Outside edge of the main landing gear door, or about 14 ft Y c.g. offset.	5	1
Pitch	0.002	273	The forward most portion of the wing structure, or about 23 ft in front of the X c.g.	5	6
Yaw	0.002	285	The forward most portion of the wing structure, or about 23 ft in front of the X c.g.	5	6

The lowest value of velocity change that can be detected is 0.0344 feet per second based on the minimum integrated acceleration (velocity) pulse size from the IMU's. In order to determine the minimum possible detectable MMOD mass for this orbiter velocity detection capability, the following assumptions were used: conservation of linear momentum, a 100% momentum transfer from the striking object, object impact at the orbiter center of mass, and a relative debris velocity of 5 nmi/sec. Based on these assumptions, the lowest detectable MMOD mass is 127 grams. From this momentum analysis, it is apparent that the orbiter being struck by an approximately one-quarter pound object (at 5 mi/sec) assuming 100% momentum transfer would most likely be noticeable by the crew. Therefore, IMU accelerometers are not considered of significant value in the search for an MMOD strike on-orbit.

4.2.2.3 Vernier Thruster Firing Algorithm

The review of orbiter data accounted for momentum changes due to VRCS jet firings. However, the possibility existed that a debris strike with enough energy or striking the orbiter at the right time could have caused the On-Orbit Digital Auto-Pilot (DAP) to command a jet firing due to a rate deadband exceedance.

The On-Orbit DAP will command jets to fire to maintain attitude errors within attitude deadbands and rate errors within rate deadbands. During periods of attitude hold, the majority of jet firings are due to the attitude deadband. Rate deadband firings typically occur at the beginning and end of attitude maneuvers, and during maneuvers due to changes in the desired rate. Figure 4-1 depicts changes in the vehicle rates due to jet firings and normal gravity gradient forces.

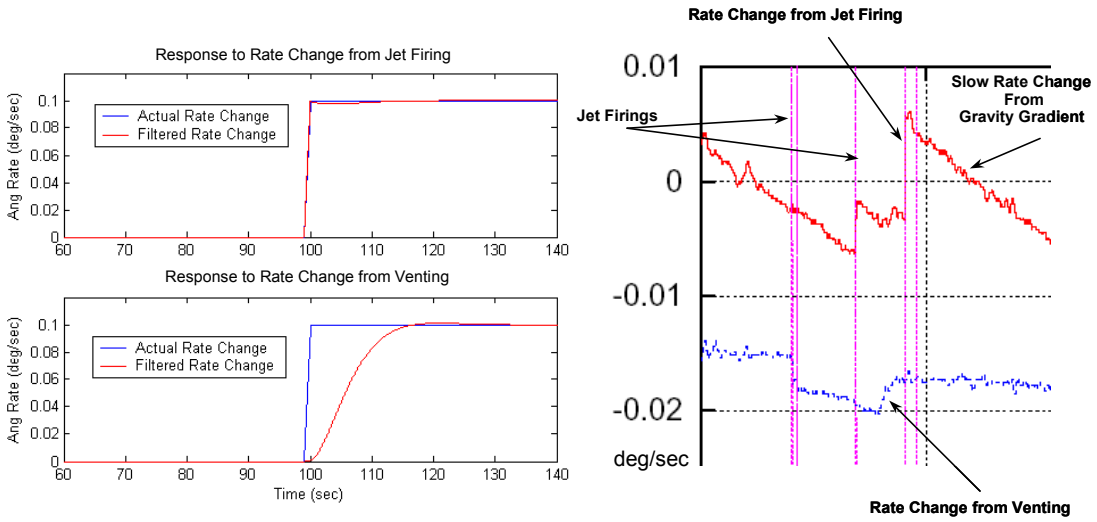

Figure 4-1. Jet firing example for vehicle rates

Analysis was undertaken to examine every jet firing and determine the cause of the firing. An algorithm was built to screen all nominal attitude deadband related firings. The remaining firings were examined to determine cause.

The algorithm assumed a VRCS jet was firing any time the downlist (telemetry) indicated a command to fire any one or more of the six VRCS jets. Also, instances of VRCS firings when the DAP attitude error (downlisted at 1 Hz) was less than 95% of the estimated attitude deadband were flagged for further investigation.

A total of 747 jet firings out of 28,779 were identified by the screening process for further investigation. Of these, 19 were due to faulty driver indications (data hits). These were verified via no change in slope of attitude rates, DAP attitude errors, and the six vernier jet fuel and oxidizer injector temperatures.

The remainder were examined and determined to be caused by (1) rate limit firings at the start and stop of attitude maneuvers, (2) rate limit firings that occurred during maneuvers due to changes in the desired rate, and (3) attitude deadband firings not screened. The final result was that there were no unexplainable jet firings in the STS-107 on-orbit data.

4.2.2.4 SAMS Data Analysis

After a review of the available payload sensors, it was determined that the SAMS data package would be the only suitable sensor that could provide additional data to aid in the detection of an MMOD strike. SAMS provides tri-axial accelerometers to measure the vibratory and transient portion of the microgravity environment. Those vibratory and transient accelerations are composed of disturbances that originate in STS equipment, scientific experiment, and crew operations. The vibratory/transient accelerations are on the order of milli-g's and are sampled at 100 Hz. While the Shuttle IMU's are designed to measure the rigid body accelerations and attitude, SAMS measures the vibratory/transient portion of the micro-gravity environment. The vibratory portion is the

dominant part of the SAMS data. Three SAMS sensor sets were aboard STS-107; however, only one had data that was downlinked during the flight. This sensor was located in the SPACEHAB Module near the Combustion Module 2 experiment.

SAMS data was used to support the aforementioned IMU rate data review. Anomalies in rates from manual review of orbiter body rates were compared to SAMS measurements to help identify sources. Figure 4-2 provides a sample plot of SAMS data and the response signature to an IMU alignment and the Enhanced Orbiter Refrigerator/Freezer (EORF) operation, as well as downlisted telemetry in the Operational Data Retrieval Complex (ODRC) system. SAMS data was also scanned for large transients to identify potential strikes (the assumption is that a hypervelocity impact would "ring" the structure). Various frequencies from nonstructural items were identified, so that they could be filtered out of the data. Figure 4-3 shows the frequency response of several items such as the EORF refrigerator and the Ku-band antenna. A detailed structural model that identifies frequencies of primary structure was developed. This model was used to screen for vibrational transients associated with orbiter wing strikes.

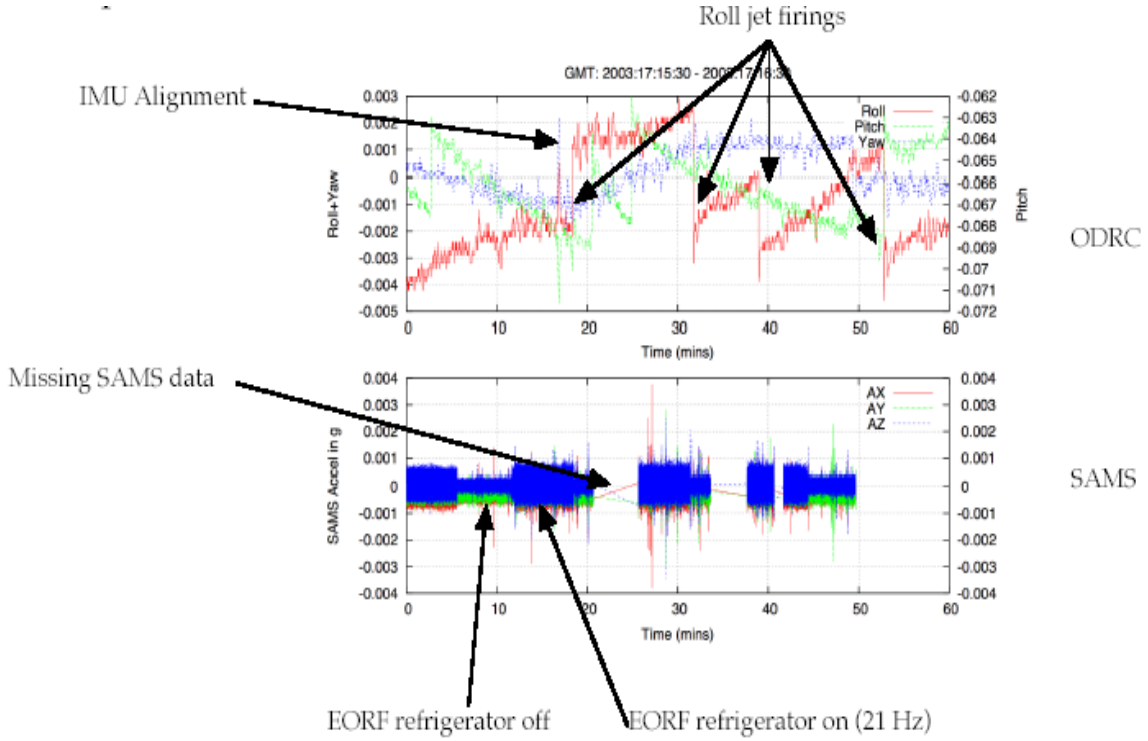

Figure 4-2. Sample data from SAMS and ODRC

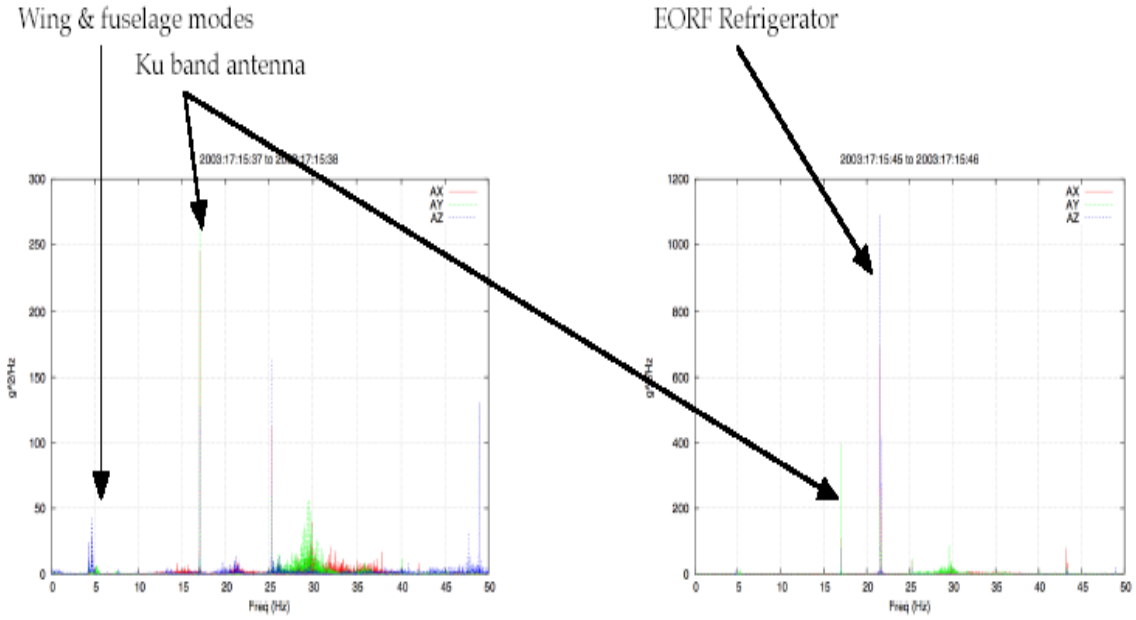

Figure 4-3. SAMS data frequency content

The review of SAMS data has not uncovered any events that could be correlated to a hypervelocity debris strike from micrometeoroids or orbital debris.

4.3 FLIGHT DAY 2 EVENT

4.3.1 Radar Tracking of Flight Day 2 Object

Air Force Space Command post-flight evaluation of radar tracking data indicated an object in the vicinity of the orbiter on flight day 2. The object remained on-orbit for approximately two and a half days, and reentered the atmosphere. Multiple government agencies participated in complex post-mission analysis of this object. These agencies include the Department of Defense Columbia Investigation Support Team, United States Strategic Command, Air Force Research Labs (AFRL) at Wright-Patterson Air Force Base, Air Force Space Command (AFSPC), Lincoln Laboratory at the Massachusetts Institute of Technology, and NASA's Johnson and Kennedy Space Centers.

The AFSPC Space Analysis Center estimated the departure time for the object was January 17, between 10:00 and 11:15 EST. Because there was no direct radar observation at the exact time of departure from the orbiter, analysis indicated that the most likely window of departure was between 10:30 EST and 11:00 EST. The analysis was complicated by the high drag profile, making it difficult to determine the precise time when the object left the vicinity of the orbiter.

The calculated departure velocity was relatively low and was estimated to be 0.7 to 3.4 miles per hour with the lower velocity being more likely. An exact departure

direction relative to the orbiter could not be determined. Multiple ground sensors including Eglin Air Force Base (AFB), Beale AFB, Cape Cod Air Force Station (AFS), and the Navy Space Surveillance fence radar tracked the object. The object reentered the atmosphere on January 19 between 20:45 EST and 23:45 EST. Figure 4-4 depicts the tracking of the object including various sensor passes.

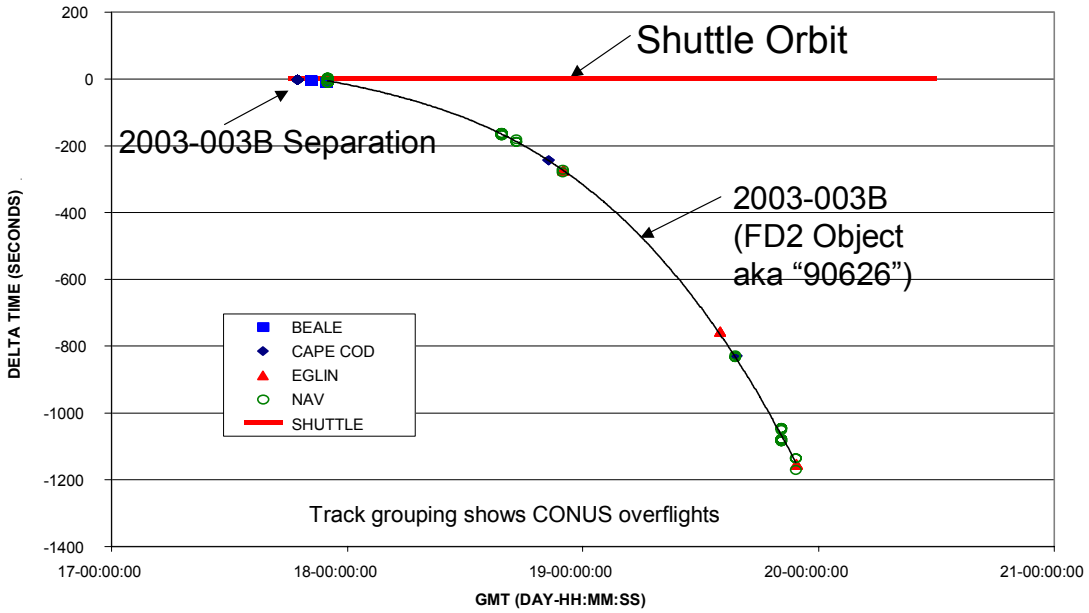

Figure 4-4. Tracking of flight day 2 object through various sensor passes

Based on the observed radar cross sections, the object appeared initially to have a minimal to no tumble/rotation rate, but it gradually developed a rate over the next two days. During a Cape Cod AFS sensor pass on January 18 at 15:29 EST, the tumble/rotation rate had a period of seven seconds. Later, on January 19 at 10:39 EST during another Cape Cod AFS pass, the apparent tumble/rotation rate had increased and the period was approximately three seconds. Figure 4-5 depicts the tumble/rotation rates during the timeframe that the object remained in orbit. The exact physical size and mass of the object are unknown, although it appeared to be a lightweight piece based on the observed ballistic coefficient.

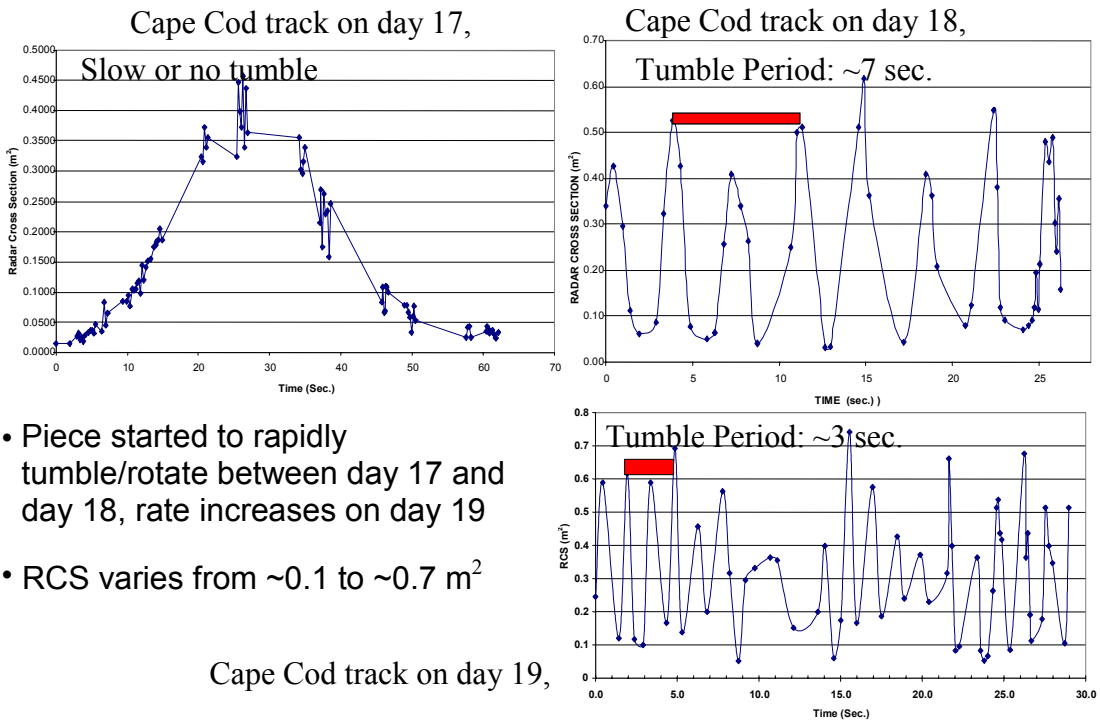

Figure 4-5. On-orbit RCS shows increased tumble/rotation rate over time

4.3.2 Analysis of Mechanisms for Object Release

The timeframe of estimated departure has been reviewed in detail. There were no unusual crew events, telemetry data, or accelerations in orbiter or payload accelerometer data that can account for the ejection of an object matching this description. SAMS, IMU, and jet firing data indicate that there was no orbital debris impact during the timeframe. Additional reviews indicate that no external mechanical systems such as the radiators or FREESTAR experiment canister doors were active during the time of interest. The port radiator was deployed on January 16 at 13:47 EST and was stowed on January 19 at 17:39 EST.

Crew commentary in the air-to-ground voice transmission during this window was routine and there was no mention of an object being observed. There was no video downlink at the time of interest, but subsequent surveys of downlinked video and still imagery did not reveal any items missing from the payload bay or visible exterior of the vehicle.

The orbiter did not perform any translational maneuvers during this timeframe. Two attitude maneuvers or orientation changes were accomplished using the small, 24 lb vernier attitude control thrusters. The first maneuver was a 48-degree yaw maneuver to a biased tail forward bay-to-earth attitude that occurred from 09:42 to 09:46 EST. Near the window of estimated departure, there was a maneuver back to the bay-to-earth tail forward attitude from 10:17 to 10:21 EST.

A manual fuel cell purge was performed later at 11:25 EST, outside the window of probable object departure. The first orbiter water dump occurred approximately two days after this event. Table 4-3 lists the chronology of relevant events.

Table 4-3. Chronology of events related to flight day 2 object

Date/Time (EST hh:mm)	EVENT
January 17 9:42 to 9:46	Attitude maneuver to a biased tail forward bay to earth attitude (biased -ZLV, -XVV)
January 17 10:17 to 10:21	Maneuver back to the bay to earth tail forward attitude (ZLV, -XVV)
January 17 10:30 to 11:00	Best estimate of object departure window
January 17 11:25	Manual fuel cell purge
January 19 16:39	First water dump
January 19 20:45 to 23:45	Object re-enters atmosphere

Data indicate that in the timeframe of the object departure there were no unusual forces or mechanisms for liberating the debris that were not also present prior to this timeframe. The orbiter had encountered a more severe loading environment during the ascent and post-insertion timeframe than on-orbit as depicted in Table 4-4. The orbiter was using the large 870 lb primary reaction control system thrusters for attitude maneuvers until the small 24 lb vernier thrusters were activated about two hours after launch. One theory is that 16 orbits of thermal cycling (day/night transitions) caused stored energy from an object in the payload bay or on the orbiter structure to be released. Another theory is that attitude maneuvers in this timeframe could have assisted the object in obtaining the opening rate from the orbiter. The data is inconclusive in determining the cause of the object departing on flight day 2.

Table 4-4. Summary of nominal launch day events

MET (hh:mm:ss)	EST (hh:mm:ss)	EVENT
0:00:00	10:39:00	Columbia launch
0:01:21.7	10:40:21.7	Foam departs ET left bipod ramp
0:01:21.9	10:40:21.9	Foam impacts orbiter left wing RCC panels 6 through 8
0:02:06.6	10:41:06.6	SRB separation
0:07:23.6	10:46:23.6	3-G throttling of Shuttle Main Engines
0:08:22.5	10:47:22.5	Main Engine cutoff command
0:08:33	10:47:33	Zero thrust
0:08:43.7	10:47:43.7	ET separation translation
0:08:57	10:47:57	Crew +X translation for ET photography
0:10:24-0:12:24	10:49:24-10:51:24	Main Propulsion System dump
0:13:44-0:14:33	10:52:44-10:53:33	Manual pitch maneuver for ET photography
0:29:52-0:34:24	11:08:52-11:13:24	Attitude maneuver to Orbital Maneuvering System (OMS)-2 burn attitude
0:41:24-0:43:24	11:20:24-11:22:24	OMS-2 burn using left and right OMS engines
~01:15:00	11:54:00	Attitude maneuver to payload bay door opening
~0:02:00	12:39	Configure for vernier attitude control (six small, 24 lb thrusters)

4.3.3 Radar Cross Section and Ballistics Testing

In addition to the careful inspection of downlinked orbiter payload bay video and still photography, radar testing and ballistics analysis of various thermal protection system items and thermal blankets have been conducted in an attempt to identify the flight day 2 object. The AFRL Advanced Compact Range Facility at Wright-Patterson AFB in Ohio tested a total of 32 items for radar cross section (RCS) at the Ultra-High Frequency (UHF) frequency of 433 MHz. These items comprise nearly the entire external surface of the orbiter as well as the exposed surfaces in the cargo bay, RCC panels, and carrier panels. The items tested also included four pieces of recovered RCC debris from Columbia to better understand the radar characteristics of partial Tee seals and RCC panels.

The results of this radar testing and ballistics analysis have excluded all external Shuttle materials with the exception of 1) a whole Tee seal, 2) a Tee seal fragment that includes an attachment flange and/or apex segment, or 3) RCC panel acreage no less than 90 square inches and roughly square in shape (+/- 20%), although curvature is possible, with a thickness on the order of 0.33 inches. An RCC panel segment matches the RCS and ballistic performance characteristics observed during the STS-107 mission.

A Tee seal fragment with an apex segment matched the RCS characteristics extremely well in any spin orientation; however, the ballistic match required a very specific spin orientation that was shown to be feasible in one analytical simulation. Therefore, it is possible that the flight day 2 object was either a partial Tee seal or RCC panel acreage piece. The Incoflex spanner beam "ear muff" insulation was also a good match for both ballistics and RCS. Because the "ear muff" is situated behind the RCC panel, it is excluded from being considered a very likely candidate because of the lack of a mechanism for exposing it to the space environment. If the damage to the wing were actually a 10-inch diameter, uniformly round hole, then an "ear muff" would be a more plausible candidate. However, it is considered unlikely that the wing damage was a 10-inch diameter round hole. The damage is considered to be the equivalent of that which would provide the same thermal response during entry as a 10-inch diameter hole did in the analyses and simulation. It is not likely that the actual wing damage was geometrically uniform. The damage was more likely a combination of cracks and holes, or a slot, such as a Tee seal or partial Tee seal missing or displaced. Therefore, the ear muff is not considered to be a good candidate for the flight day 2 object. Figure 4-6 shows the three leading edge components that match both RCS and ballistics analysis. It should be noted that a full Tee seal and RCC panel are shown in these photos while there are specific partial Tee seal and RCC panel configurations that match the test results.

Reinforced Carbon-Carbon (RCC)
Leading Edge Panel (Flight Hardware)

Incoflex "Ear Muff" Spanner Beam
Insulator

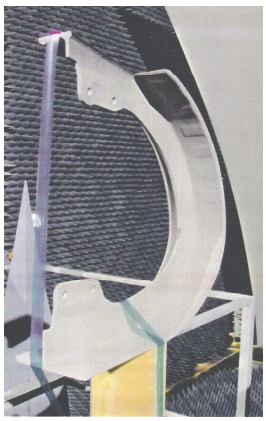

Reinforced Carbon-Carbon
(RCC) T-Seal

Figure 4-6. Leading edge structural subsystem components matching RCS and ballistics

4.3.4 KSC Lost and Found Items

A review was conducted of the lost-and-found items from the Columbia processing flows of STS-107, STS-109, and the last Columbia OMM-J3. The largest tools that were lost and not found are listed in Table 4-5; other smaller items (e.g., washers and nutplates) are not listed. The item, size, location, and Problem Report (PR) number are noted. The largest item documented on a Lost and Found (LAF) PR is a piece of a blanket 6" x 3" lost in the payload bay (LAF-2-27-0611) during STS-109 processing. These items were screened using the ballistic coefficient and RCS criteria. All of the items failed the RCS screening and their RCS is too low to be a candidate for the flight day 2 object.

Table 4-5. Lost tools in Columbia processing for STS-107, STS-109, and OMM J3

Processing Flow	Tool Description	Location	PR #
OMM J3	Allen Socket, 2"x 1/2"	Mid-body	(LAF-2-J3-0550)
OMM J3	Plastic Extraction Tool, 22 gage	Flight Deck	(LAF-2-J3-0567)
OMM J3	Pliers, 7 3/4"	Hypergolic Maintenance Facility (HMF)	(LAF-RPO5-15-0004)
OMM J3	Screwdriver, 11"	HMF	(LAF-RPO5-15-0005)
OMM J3	Screwdriver, 7"	HMF	(LAF-RPO5-15-0006)
OMM J3	Screwdriver, 8"	HMF	(LAF-RPO5-15-0007)
STS-109	Mini Flashlight, 6"	Forward Reaction Control System (FRCS) 2	(LAF-FRC2-27-0005)
STS-107	Socket, 7/16"x 5/16"	Aft Compartment	(LAF-2-28-0632)

4.4 ORBIT SUMMARY

Extensive data review provided no conclusive indication of damage from either the ascent foam impact or an MMOD hypervelocity impact based on orbiter telemetry, crew downlinked video and still photography, or crew reports.

Orbiter IMU and jet firing data have been reviewed, and this review confirmed that the IMU's were not designed for MMOD detection and data available to detect an MMOD strike is coarse. This data review found 13 events that required additional analysis. After this additional analysis, only two events remained that could not be ruled out as MMOD strikes. An examination of all VRCS jet firings was conducted and showed no unexplainable jet firings during STS-107.

SAMS data were also used in the analysis of the 13 events detected using IMU rate data. SAMS sensor data were also screened for large transients indicative of an MMOD strike; however, none were found. A model was developed that identifies the modal frequencies of the Shuttle structure (including wing modes) to further screen of the SAMS data for MMOD strikes.

A review of the flight day 2 event has been performed including RCS testing and ballistics analysis of 41 items, including TPS. The analysis performed to date indicates that a full Tee seal, a partial Tee seal, and RCC panel are the only tested items that have not been excluded.

It is possible that another untested object could match the RCS and ballistics and have departed the orbiter on flight day 2. Objects have departed the payload bay on previous Shuttle missions. The data are inconclusive as to whether the ET ascent foam debris event and the flight day 2 event are related.